5-2020

Effects of Incubation Temperature on Nanomechanical Properties of β-Lactoglobulin Amyloid Fibers

Santosh Khatri
The University of Texas Rio Grande Valley

EFFECTS OF INCUBATION TEMPERATURE ON NANOMECHANICAL PROPERTIES OF β-LACTOGLOBULIN AMYLOID FIBERS

A Thesis

by

SANTOSH KHATRI

Submitted to the Graduate College of
The University of Texas Rio Grande Valley
In partial fulfillment of the requirement for the degree of

MASTER OF SCIENCE

May 2020

Major Subject: Physics

EFFECTS OF INCUBATION TEMPERATURE ON NANOMECHANICAL PROPERTIES OF β-LACTOGLOBULIN AMYLOID FIBERS

A Thesis
by
SANTOSH KHATRI

COMMITTEE MEMBERS

Dr. Ahmed Touhami
Chair of committee

Dr. Nikolaos Dimakis
Committee Member

Dr. HyeongJun Kim
Committee Member

May 2020

ABSTRACT

Khatri Santosh, Effects of Incubation temperature on the fibrillation of amyloid β-lactoglobulin amyloid fibrils. Master of science (MS), May 2020, 55 pp., 20 figures, references, 49 titles

Apart from pathological connection to neurodegenerative disease, amyloid fibrils derived from food protein can also be used as biomaterials in nanotechnology, material science and food science because of their extremely strong, highly ordered and organized fibers. The purpose of this thesis is to study and compare the mechanical properties of β-lactoglobulin (β-lg) grown at different incubation periods using AFM Peak Force QNM Mode. Average moduli of elasticity of β-lg fibrils incubated for 24 h, 48 h and 72 h were measured to be 8.6GPa, 5.7GPa, and 4.7GPa respectively. In addition to the average dimensions of the fibers and their monomers, their persistent lengths were determined as well using FiberApp software. Our data showed that β-lg fibers incubated for longer time are more flexible compare to one grown at 24 h. However, the average dimensions of the fibers remained similar. We believe that this study is another step to better understand the mechanism of assembly of amyloid fibers which is essential for combating amyloid diseases as well as exploiting the potential benefits of protein/peptide design

ACKNOWLEDGEMENT

First, I would like to thank my advisor and teacher Dr. Ahmed Touhami who gave me the opportunity to start this journey in his laboratory. I am grateful for his kindness, advices, personal support and for how he had taught me to face Research with independent and curious full attitude. This is what makes me in love with science and makes me work hard to complete my thesis and earn the degree.

I also would like to acknowledge my committee members, Dr. Nikolaos Dimakis and Dr. HyeongJun Kim for spending time in reading and correcting this thesis. I also would like to offer my heartfelt thanks to all the members of single-molecule Biophysics lab at UTRGV for helping and providing me the peaceful environment to conduct the research and study well within the lab. Last but not the least, I would like to express my sincere graduate to all the personages including my friends, faculty members of the UTRGV, whose active guidance, help, cooperation and encouragement help me to complete this project and make it full success.

TABLE OF CONTENTS

Page

ABSTRACT iii

ACKNOWLEDGEMENT iv

TABLE OF CONTENTS v

LIST OF FIGURES vii

CHAPTER I. INTRODUCTION 1

1.1. Amyloid Fibril 1

1.2. Amyloid fibril formation mechanism 2

1.3. Structure and properties of Amyloid fiber 3

1.4. Amyloid fiber from food proteins 5

1.5. Techniques used to characterize amyloid fibers 5

1.6. Objective of the Thesis and Synopsis 6

CHAPTER II. MATERIALS AND METHOD 7

2.1. β-lactoglobulin structure 7

2.2. Atomic force Microscopy (AFM) 8

2.3. Peak Force Quantitative Nanomechanical Mode (QNM) 10

2.4. Analyzing tools and Software 12

2.4.1. FiberApp 12

2.4.2. WSXM software 13

2.5. Sample Preparation 13

2.6. Experimental settings and Measuring environment 14

2.7. Persistent length and polymer chain model 16

CHAPTER III. RESULT AND DISCUSSION 20

3.1. Synopsis 20

3.2. Imaging at different Incubation time 20

3.2.1. Statistical analysis of fiber Height 22

3.3. Mechanical properties of the fibers 24

3.3.1. Nanoscale ordering of β-lg fibers: Dimension of each monomer 24

3.3.2. Peak force QNM Measurement of β-lg fibers 25

3.3.3. Changes in mechanical properties during fibrillation process 29

3.3.4. Bending stiffness quantification: Measurement of persistent length 35

3.3.5. Identical Moduli of elasticity of different polymorphic forms of fibril 37

3.4 Discussion 40

CHAPTER IV. CONCLUSION AND FUTURE PROSPECTIVE 44

REFERENCES 47

BIOGRAPHICAL SKETCH 55

LIST OF FIGURES

Page

Figure 1 Amyloid fiber formation (Lambrecht et al., 2019) 3

Figure 2. Structure of amyloid fiber (MC Bewley, 1997) 4

Figure 3. crystal structure of one monomer of β-lg (Loveday & Sawyer, 2016) 7

Figure 4 An illustration of the fundamental principle of AFM. (Cappella & Dietler, 1999) 9

Figure 5 Bruker Bioscope Atomic Force Microscope used in the present study.....10

Figure 6 Plot of z-piezo position and force as a function of time (Cao & Mezzenga, 2019) ..11

Figure 7 Basic Force-separation curve recorded in QNM (Claesson et al.,2017) 14

Figure 8 Diagram of indentation models used in Peak force QNM 15

Figure 9 R and L represent the end to end distance and counter length of the polymer.....18

Figure 10 AFM height images of β-lg fibers prepared at different incubation time 21

Figure 11 Statistical distributions of the heights of β-lg fibers for the 3 incubation times 23

Figure 12 AFM-cross sections on single β-lg monomer showing the dimensions of single monomer for each incubation time.....24

Figure 13 QNM measurements on the β-lg fibers grown at 24 h 26

Figure 14 QNM measurements on the β-lg fibers grown at 48 h. ……. 27

Figure 15 QNM measurements on the β-lg fibers grown at 72 h. ……. 29

Figure 16 Statistical distributions of the Young's modulus calculated from the QNM at each incubation time based on DMT model 31

Figure 17 Statistical distributions of the deformation parameter calculated from the QNM at each incubation time 33
Figure 18 Histograms summarizing Young's Modulus and deformation measurements for the three-incubation time 34
Figure 19 Graphs of mean square-end-to-end vs counter length of β-lg fibers at the different Incubation time 37
Figure 20 AFM height images showing three different polymorphic forms of β-lg fibrils observed in fibers incubated for 24h 39

CHAPTER I

INTRODUCTION

1.1. Amyloid fibril

The term amyloid fibril was first coined in 1854 by German laboratory Physician Rudolph Virchow, while studying the abnormal deposit within the brain (Rud et al., 1851). He discovered that Corpora amylase, on treating with iodine turned into blue marks while it turns out to be violet upon addition to sulfuric acid. This is the specific characteristics of cellulose. So, he concluded that these deposits in the brain are cellulose and named it 'amyloid' which is derived from Latin word 'amylum' meaning 'starch like'. Amyloid fiber are self-assembled, insoluble protein fibrils which are aggregated from globular proteins under certain physiological conditions. Such irreversible fibril formations of various proteins are connected to disorders such as Alzheimer's, Creutzfeldt-Jakob and Huntington's diseases which is still not fully elucidated (Rud et al., 1851; Wei et al., 2017).

Amyloid aggregation is a form of biological mechanism of protein unfolding and self-assembly that has significance in many of fields such as medicine, biology, material science. It has also been a hot topics of research because of its implication in neurodegenerative disorders (Wei et al., 2017). 40 or 42-residue peptide also called amyloid-beta protein gets deposited in brain and around cerebral walls in the form of amyloid plaque (Glenner & Wong, 1984). Aggregates of lewy bodies contained within the neuronal cytoplasm of substantia nigra inside the brain of patients of Parkinson disease contains protein alpha-synuclein as major component

(Osterhaus et al., 1997; Trojanowski & Revesz, 2007). Similarly, extranuclear deposit of huntington protein is the major component in Huntington Disease (DiFiglia et al., 1997). Amyloid have also been found in many physiologically beneficial roles like adhesive and hormone storage (Volpatti & Knowles, 2014). Bacteria, like Salmonella, *Escherichia coli*, and algae utilize functional amyloid to modulate surface adhesion (Mostaert et al., 2006). More than 30 human peptide granules have been discovered so far that are stored in amyloid-type granules for long term use (Maji et al., 2009). These granules could be translated to a system to overcome short-term delivery problem of drugs enabling amyloid as controlled drug release system (Trojanowski & Revesz, 2007). Finally, the nonlinear optical properties of ultrashort amyloid-like peptide hold good promise for new bioimaging application as they have cytotoxic effect to human cell and easy to observe within the cell even without florescence labelling (Ni et al., 2019).

1.2. Amyloid fibril formation mechanism

The amyloid fiber formation takes place by aggregation of protein under acidic condition. Under the variation of environmental conditions (pH, temperature, incubation time) protein monomer becomes unstable and starts to unfold partially which further interacts with other partially unfolded monomer (de Jongh & Broerse, 2012; Ohnishi & Takano, 2004). The repeated sequence of partially unfolded monomer with high hydrophobicity, exposed amide N-H group and C=0 forming H-bonding bind to serve as template for fibrillation process (Ohnishi & Takano, 2004). Once the oligomer is formed, one theory suggested that unfolded monomer attach to each other by end to end (Sozer & Kokini, 2009), while a second theory proposed that nuclei self-assemble each other to form the protofibril (Ross & Poirier, 2004). As shown in figure 1, these protofibrils after certain length gets assembled into mature amyloid fibrils which just laterally

associate and align prior to twisting into mature fiber (Adamcik & Mezzenga, 2012) . However, in some cases, the growth of the protofibrils is not completed because of the formation of the loop (Lambrecht et al., 2019).

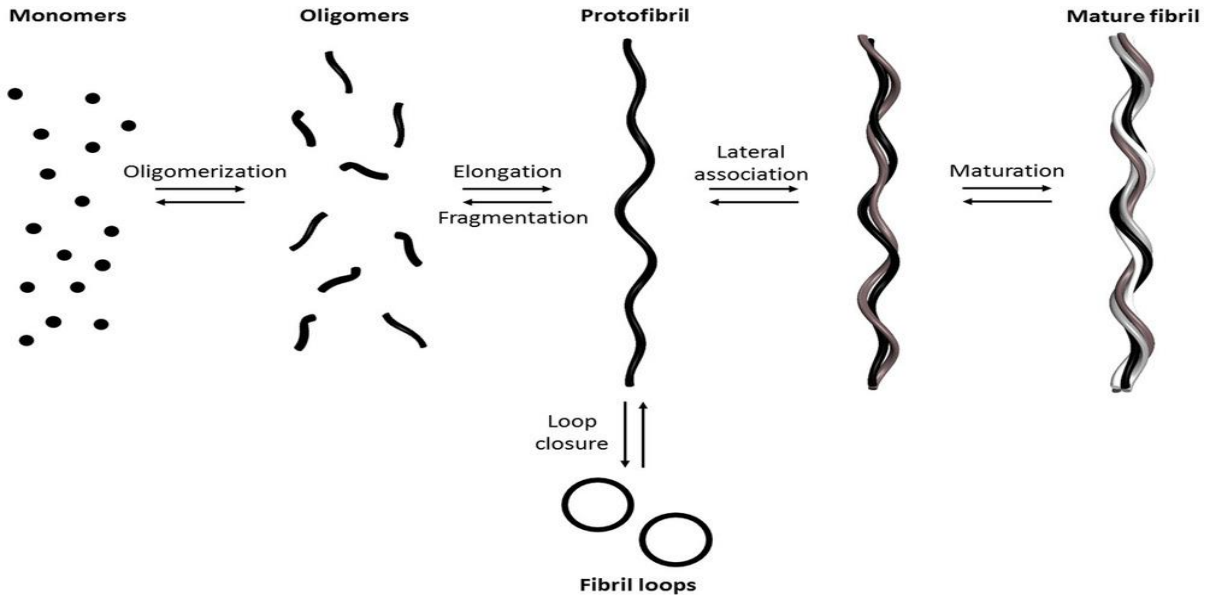

Figure 1. Amyloid fiber formation: initiating fibrillation from monomer to protofilament and finally to mature fibrils and the mature protofilament formed by fibril loop (Lambrecht et al., 2019).

1.3. Structure and properties of amyloid fiber

Both intrinsic properties such as amino acid composition, hydrophobicity and the extrinsic properties such as temperature, incubation time, pH, ionic strength are the factors that affect morphology of proteins aggregates (Zapadka et al., 2017). Most of studies focused on the morphological properties like fiber length, height and twisting characteristics (Petkova et al., 2016). Different classes of amyloid fibrils share common 2-6 or sometimes more protofilaments with 2-5 nanometer diameter and length from 100 nm-16 micrometer long (figure 2) (Adamcik &

Mezzenga, 2011). These protofilaments twist or coil together and are characterized by core cross-beta sheet which are stacked by hydrogen bonding in the direction perpendicular to its long axis. Since the structure has its relationship with different nanomechanical properties of fiber, some study has also focused on the polymorphism characteristic of amyloid fibrils which is the form having different structural features (Paravastu et al., 2008). The biological significance of amyloid polymorphism is that it can be a molecular basis for prion strain. A synchrotron X-ray study in 1997 showed that amyloid fibrils of six different proteins with 6 different clinical syndromes share the same beta-diffraction architecture (Sunde et al., 1997). Mechanical and textural characteristics present in the fibrils are the properties that are targeted for medical and nanotechnological applications (Wang et al., 2010).

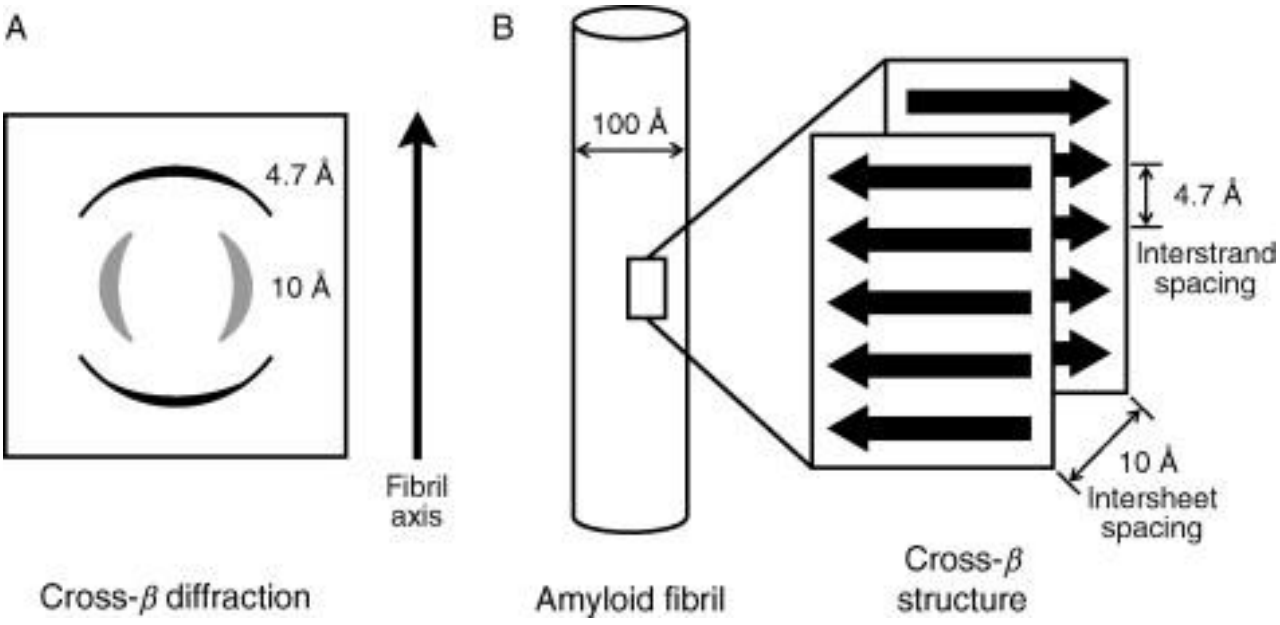

Figure 2. Structure of amyloid fiber(MC Bewley, 1997)

1.4. Amyloid fiber from food proteins

Proteins are present as major components in many food components; ovalbumin is a major protein in egg white, serum albumin present in red meat, β-lactoglobulin in bovine milk. Protein aggregation in food has been studied for many years because of the implication of aggregated protein-amyloid protein to neurogenerative disease (Ha & Zemel, 2003). In addition to having the connection to neurodegenerative diseases, amyloid fibers derived from food proteins can also be used in variety of fields such as biomaterial, biomedicines, and nanotechnology (Wei et al., 2017). The amino acid present in food protein provides the nutritional basis and their derivatives help in the structural formulation of the food products (gelling agents, binding agent for fat, thickening agents) (Biancalana & Koide, 2010; Riek & Eisenberg, 2016).

1.5. Techniques used to characterize amyloid fibers

Despite having flexible structural polymorphic fibrils, amyloid fibers share similarities at the atomic level called cross-β sheet which are parallel to each other but with individual β-strand within the same β-sheet perpendicular to fibrillar axis. The techniques that are used to identify and characterize the amyloid fibers depend on the distinctive structures that the fibers have. Although the X-ray diffraction is the classical standard method to illustrate the cross-β structure (Zandomeneghi et al., 2009), the Thioflavin (ThT) fluorescence, nowadays, are widely accepted as the best method to show the cross-β structure as it has high selective binding to amyloids (Micsonai et al., 2015). The other techniques that are used to identify the cross-β structure are circular dichroism (CD) and Fourier transform infrared spectroscopy (FTIR) (Petkova et al., 2002). The structure of the amyloid at atomistic level are studied by solid-state magnetic resonance (NMR), cryo-electron microscopy but these are limited to few pathological amyloid fibers (Pittenger et al., 2010). The molecular weight of the peptide molecules is estimated by mass

spectroscopy. Similarly, the kinetics of the fibrillization is observed by the dynamic light scattering (DLS), florescence spectroscopy of intrinsic fluorophores (Riihimäki-Lampén et al., 2010). The peak force atomic force microscopy (Peak-Force AFM) is one of the most recently used technique to investigate structural and mechanical properties of amyloid fibers at the single fiber level and under various conditions.

1.6. Objective of the thesis and synopsis

The goal of this thesis is to determine the nano structural and nanomechanical properties of amyloid fibrils composed of β-lactoglobulin protein at different duration of incubation time, constant temperature, and fix acidic pH. These properties are investigated using high-resolution AFM imaging and AFM-peak force quantitative nanomechanical mode (QNM). we focused on the quantification of nanomechanical properties such as young's modulus of elasticity, adhesion, deformation. The fibers were grown under similar conditions at 80 ^{o}C and for three different time durations (24, 48, and 72 hours). The AFM measurements were performed under similar conditions for all the studied fibers. The objective is to investigate how the different incubation period affects the structural and nanomechanical properties of the amyloid fibers.

CHAPTER II

MATERIALS AND METHODS

2.1 β-lactoglobulin structure

β-lactoglobulin (β-lg) is found in milk of many mammals, specially found in whey group of ruminant milk at the concentration 0.2-0.3 g/100 ml (Ban et al., 2006; Gosal et al., 2005) but completely absent in human, rodent and lagomorph milk. It is a member of lipocalin family which has similar common structure and exhibit high affinity for hydrophobic molecules, especially act as transporter of retinol (Cappella & Dietler, 1999). Two main structural properties of β-lactoglobulin have made it as a model for protein studies. First, β-lg with large molecular size helps to understand the principle of denaturation, aggregation of protein and binding ligand having small hydrophobic molecules. The second factor that made β-lactoglobulin an archetypal protein for several biophysical studies like folding and protein aggregation, is its abundance and easy purification (Usov et al., 2013).

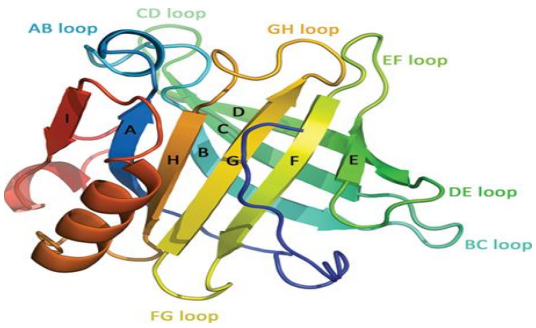

Figure 3. crystal structure of one monomer of β-lg (Tai et al., 2016)

Figure 3 illustrates a crystallographic structure of a β-lg monomer. β-lactoglobulin contains 162 amino acid residues which include two disulfide bonds (Cys 66-Cys160 and Cys106-Cys119) and a free thiol (Cys 121) that shows pH dependent activity. β-lactoglobulin has a molecular weight of 18.4 kDa and two genetic variant A and B different in two amino residues; Asp 64 and Val 118 in variant A and Gly and Ala in variant B (Zsila et al., 2002). β-lg is composed of 8 strands of antiparallel sheet (A-H strand) which coil round beta-barrel. It is bordered with 3-turn α-helix (between H and G strands). The β-strands A-H of β-lg is connected by seven loops; namely AB, BC, CD, DE, EF, FG and GH. The ninth strand (I) helps to form the dimer interface at neutral pH (Riihimäki-Lampén et al., 2010). The closed ends BC, DE, and FG are a bit shorter with more rigidity than the open ends AB, CD, EF, and GH (Sakurai et al., 2009). The loop EF acts as the gate over the binding site. Although the central calyx with hydrophobic residue scattered around it, is considered as the ligand-binding site(Ohnishi & Takano, 2004), some study also claim more secondary binding points (second site involving the residue Trp19, Tyr 20, Tyr 42, Gln 44, Gln 59, Gln 68, Leu 156, Glu 158 and His 161 and third site involving residue Tyr 102, Leu 104, and Asp 129) (Zsila et al., 2002).

2.2. Atomic Force Microscopy (AFM)

In 1986 a Nobel prize in Physics was shared by G. Binning and H. Rohrer for their invention of scanning tunneling microscope with the findings that it can image individual atoms with high degree of precession. Winning with his colleague, C. Gerber and C. Quate calculated the force between two individual atoms and found that they can easily make the cantilever weaker than the equivalent spring between two atoms. Relying on this idea the scanning tunneling microscope led to the advancement of a host of scanning probe microscope which depends on

scanning of a sharp tip over sample surface and called Atomic Force Microscope (Flower et al., 2000). As shown in figure 4A, AFM with very sharp tipped cantilever scans over a sample surface. As the tip approaches the surface, attractive force between surface and tip comes into play and causes the cantilever to deflect towards surface (figure 4B). When the tip comes closer and closer to the surface, the predominant repulsive force causes the tip to deflect away from the surface. The incident laser beam is reflected off the top of the cantilever and monitored by a position sensitive photo diode (PSPD). The height of the tip above the sample is controlled by a feedback loop.

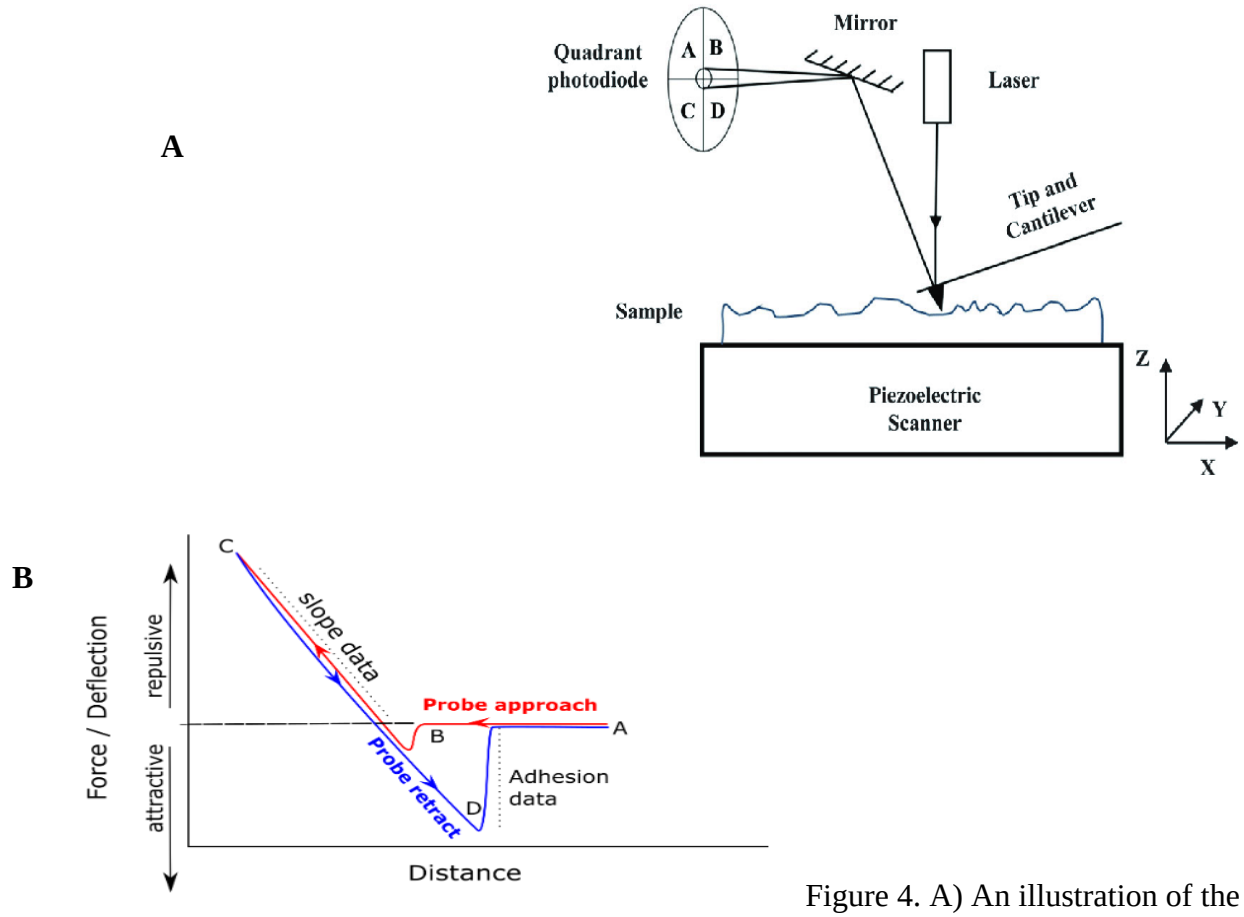

Figure 4. A) An illustration of the fundamental principle of AFM. B) A schematic of AFM force distance profile (Cappella & Dietler, 1999).

The force-distance curve as shown in the figure 4B illustrates the difference between two data sets recorded during tip approach (blue) and tip retract (red). Cantilever acts as a Hook-spring whose stiffness (k) can be measured with the deflection of the cantilever. The force (F) acting on the cantilever can be calculated as $\mathbf{F = k \times d}$. The mechanical measurement on any sample can be performed by simply pushing the AFM tip against the sample surface and recording the resulting force-distance curve.

Figure 5. Bruker Bioscope Atomic Force Microscope used in the present study. The AFM is combined to an inverted fluorescence microscope

2.3. Peak Force Quantitative Nanomechanical (QNM)

The recent improvement in noise reduction, data acquisition, speeding data led the manufacturer (Bruker, AXS, California, USA) of AFM to develop Peak force Quantitative

nanomechanical (QNM)-Mode. Peak force QNM-Mode is considered as one of the potential high-resolution technique to determine the structural feature and associated nano mechanical properties of amyloid fiber (Kalapothakis et al., 2015). Peak force QNM-Mode is an extended version of peak force tapping mode empowering us in quantitative measurement of nano-scale materials properties like modulus, adhesion, deformation and dissipation. The controlled force applied on a sample with the use of variety of probe have facilitated high resolution imaging without damaging the sample. The measurement is more accurate with lowest possible uncertainty because of the combination of peak force QNM, geometry of the tip and frequency calibrated probe. The peak force QNM can investigate the quantifiable mechanical properties like modulus of elasticity in the range of 1KPa to 100GPa.

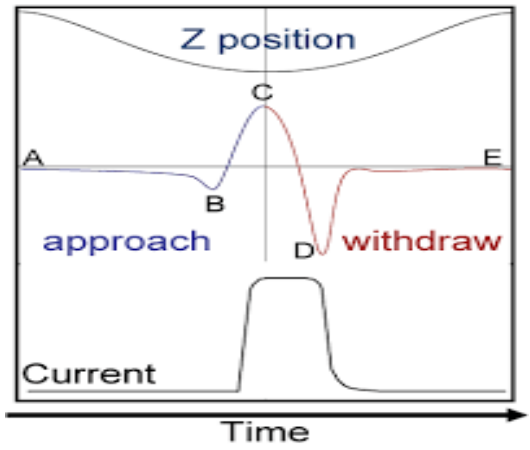

Figure 6. plot of z-piezo postion and force as a function of time with jump to cantact (B), peak force (C), Adhesion (D) (Cao & Mezzenga, 2019)

Figure 6 exhibits the position of z-piezo when the tip of the cantilever with respect to the position of the sample. The force-time curve of the system can be converted into force-distance curve using calibrated scanner setting. The line at the top of the figure 6 illustrates the z-position

modulation for one period as function of time. The lower solid line represents measured force on the probe when the probe approaches or moves away from the sample. The solid line with blue part from A to C represents the force on the probe when the tip approaches the surface whereas the blue line from C to E represents the force on the probe when the tips moves away from surface.

2.4. Analyzing tools and software

2.4.1 FiberApp

FiberApp is an analyzing tool works under the cascade of algorithm which explore and quantify the topological feature of fibril-like objects. Images from any microscopy sources like AFM, SEM, Optical, and fluorescence can be analyzed with this software. It is an open-source code written in MATLAB programming language cascading algorithm based on statistical polymer physics concepts. The tracking procedure of the software is based on the A* pathfinding algorithm followed by the active contour model, displaying graphical output which allow the tracking of thousands of filamentous and synthetic objects in a short time. The major output features of FiberApp are height, length, bond and pair correlation function, mean-squared end-to-end distance, mid-point displacement, 2D order parameter, kurtosis, fractal exponents, discrete Fourier transform, orientation, curvature and kink angle (Usov & Mezzenga, 2015). Some fibrillary-like structures and their feature have been investigated using FiberApp software. For example, the six different polymorphic types of the Serum Albumin Bovine fibrils with two flexible (1 left handed, 1 right handed) and 4 intermediate, have been identified using FiberApp (Usov et al., 2013). The rigidity and mechanical properties of functionalized multiwalled carbon nanotubes with sulfonic groups were also investigated with the help of this software (Li & Mezzenga, 2012).

2.4.2 WSXM software

Each AFM microscope comes with its own analyzing software that allow for basic imaging and force curves processing. However, some advanced analysis requires more flexible and powerful software. One of them is called WSXM program that is widely used by AFM community and designed to work under MS-Windows. WSXM is able to read all type of AFM data and is divided into data processing and data acquisition parts. In this study most of the image processing were performed using WSXM and all the QNM analysis were completed using the original AFM software called Nano scope Analysis.

2.5. Sample Preparation

β-lactoglobulin was obtained from Sigma-Aldrich. 2 wt. % solution was prepared by dissolving the powered form of β-lactoglobulin in Milli-Q water at room temperature for at least an hour. The solution was further centrifuged at the rate of 2800 rpm with the orbit of 4 mm using Labdoctor mini Vortex centrifuge, adjusted to pH 2, and filtered through the 0.45-μm Millipore filter before heat treatment. 20 ml of the β-lg solution were put in 50 mL conical centrifuge tube, which was hermitically sealed, and placed in a water bath at 80 ^{o}C for about 24 hours. After the heat treatment, the tube is immediately cooled by immerging it into mixture of ice and water for 30 min to hasten the aggregation process. Only a small amount of the sample was taken out and diluted 10 times (0.2% wt, in Milli-Q water) in order to observe the individual fibers. To prepare the sample for AFM measurements, few drops (~ 30μl) of the diluted solution were poured into a freshly cleaved mica surface slide and allowed to dry in air between 15-30 min. Similar process was repeated for more incubation time period of 48 hours and 72 hours respectively. AFM measurement were carried out using both imaging and peak force QNM modes for all samples.

Sample preparations and measurements were repeated at least three times for each incubation temperature. Data analysis were performed using all three software WSXM, FiberApp, and Nanoscope Analysis.

2.6. Experimental settings and Measuring environment

In Peak Force QNM mode, the cantilever oscillates at a frequency lower than its resonance called Tapping mode frequency. The maximum force applied by the tip, also called peak force, is controlled and used as a feedback parameter (figure 7). For all the QNM measurements, the Bruker RTESP Antimony doped Si AFM cantilevers with no coatings on both sides, resonance frequency of 300 KHz, nominal spring constant of 40 N/m and tip radius of 8 nm were used. The scanning rate was attuned to 1 Hz (1 line/s). All the measurements were performed using QNM mode in air and at room temperature

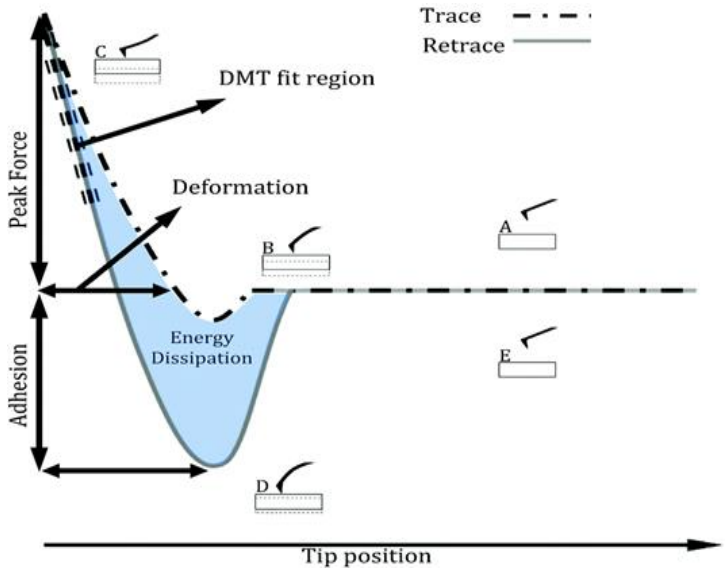

Figure 7. An illustration of the basic Force-separation curve recorded and used in QNM mode to extract the mechanical properties of the sample (Claesson et al., 2017)

The force-separation curve indicating the peak force tapping operation and tip trajectory in one complete cycle is given in figure 7. It illustrates how the periodically modulated probe interact with the surface. These force curves can be captured at any location and time during scanning using the 'High-speed data capture' function. The recorded forces are analyzed and fitted using well known models as discussed below. Different type of mechanical properties such as, elastic modulus, adhesion, dissipation and deformations of the sample are obtained.

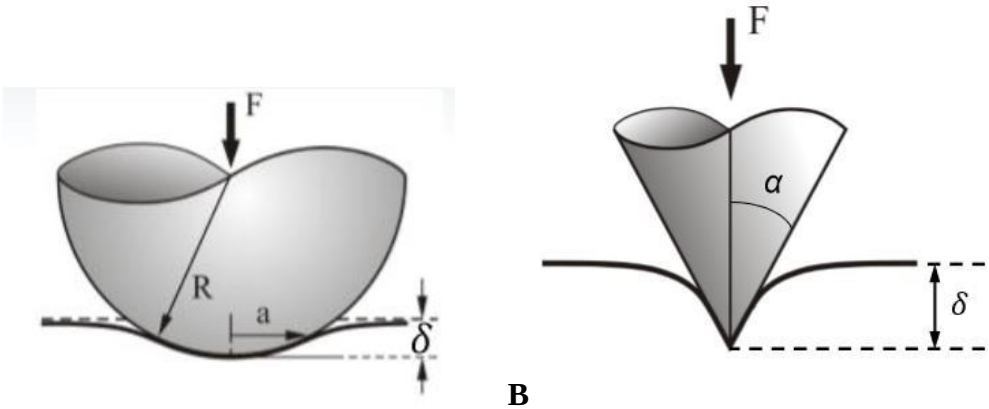

$$F = \frac{4}{3}\frac{E}{(1-\nu^2)}R^{1/2}\delta^{3/2}$$

$$F = \frac{2}{\pi}\cdot\frac{E_s}{1-\nu_s^2}\cdot\tan\alpha\cdot\delta^2$$

Figure 8. Diagram of indentation models used in Peakforce QNM: A) the Derjaguin-Muller-Toporov (DMT) model deduces the Young's modulus E of the sample using deformation δ data and tip radius R. B) is the Sneddon model, where α is the half angle of the indenter (tip). Tip radius is a required parameter for calibration in QNM(Hua & Ph, 2014)

The Peak Force QNM uses two models to deduce the modulus of elasticity; DMT model and Sneddon model depending upon the nature of the tip used for indenting the surface. Figure 8a, represents the Derjaguin-Muller-Toporov (DMT) Model, which is one of the main theoretical

models used to calculate the young's modulus of elasticity of the sample when indenter used has a spherical shape (a glass bead), with radius R and deforms the sample by δ(Hua & Ph, 2014). Figure 8b, is an illustration of Sneddon Model which can be used when the indenter has a conic shape, the angle of indentation α, and the deformation of the sample δ are known (Hua & Ph, 2014). In our measurements, the deflection sensitivity of the sample was first calibrated using the force measurements on fused silica sample. The spring constant was calculated to be 45 N/m using 'thermal-tune' method. The tip radius of the AFM tip was calibrated using a model called contact mechanics using a sample with known elastic modulus. The modulus of elasticity was obtained by fittings of real-time curve using the Derjaguin-Muller-Toporov (DMT) model. DMT model can be regarded as the modified version of Hertzian model which considers the adhesive force between tip and the surface while maintaining the area of contact. Thus, it works well with hard samples and low penetration depth.

2.7. Persistent length and polymer chain model

The polymer conformation changes when it transits from 3-D to 2-D space. This reduction in one-degree of freedom constraints the configuration of the molecule. Thus, the interaction between the polymer and a given surface causes the molecule to adopt one of two possible conformations. The molecule can either freely equilibrate on the surface or adhered to the surface before being equilibrated. Thus, the conformation of the molecule at the 2-D surface provides meaningful information about its structural and mechanical properties of the molecules.

The persistent length, which is the measure of the molecule length over which the direction of the polymer chain stops persisting, is the basic parameter that characterize the stiffness and mechanics of the polymer chain like, protein, DNA molecules. For polymer with longer contour

length the persistent length appears to be flexible, a polymer with shorter contour length the persistent length is rigid, while a polymer with a counter length equal to the persistent length is semi-flexible. The FiberApp software is used in the present study to determine the persistent lengths of the β-lg fibrillary structures based on the mean-square end -to -end distance, $<R^2>$, of the fiber extracted from the AFM images (Krathy and Porod, 1949).

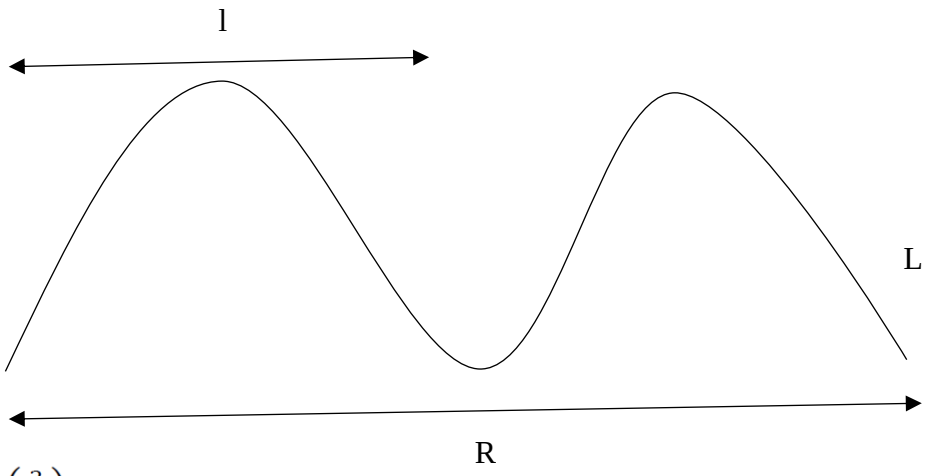

$$\langle R^2 \rangle = \left(\frac{2}{\lambda^2}\right)(\lambda l - 1 + \exp(-\lambda L))$$

(A)

(B)

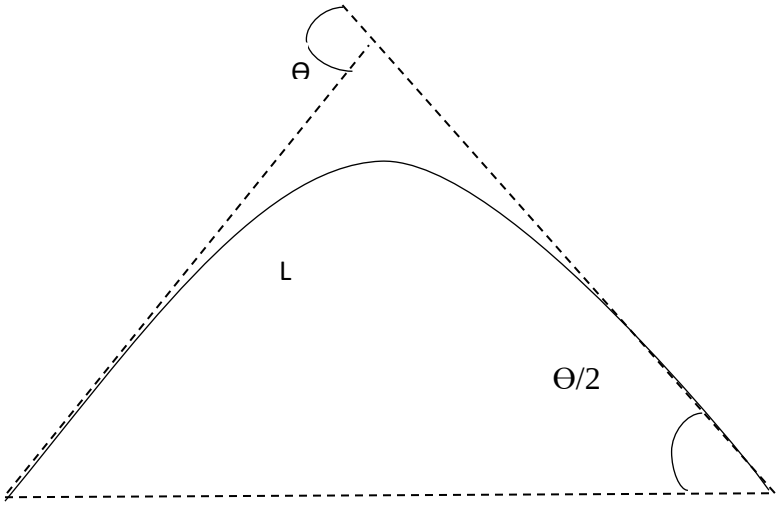

Figure 9. R and L represent the end to end distance and counter length of the polymer. λ is equal to 1/Lp. In this thesis the equation of $<R^2>$ is fitted to data obtained from AFM images of fibrils to determine persistence length Lp.

The Figure 9 relates the cosine of the angle Θ of successive segment of the chain of polymer with the persistent length Lp and contour length L of the polymer. The macroscopic quantities such as energy, moment of inertia can be related to the persistent length of the polymer, Lp(Broedersz & Mackintosh, 2014).

$$E \times I = k_B \times T \times Lp \qquad (1)$$

According to concept of polymer physics, energy required to bend the two segments of the polymer by an angle Θ separated at distance 'l' is given as, (54)

$$E = Y \times I \times \Theta^2 \times /2l \qquad (2)$$

The normalized probability density function for angle Θ is obtained as,

$$<P(\Theta)>_{2D} = \sqrt{\frac{\lambda p}{2\pi l}} \exp\left(-\frac{\lambda p \theta^2}{2l}\right) \qquad (3)$$

The cosine of the angle of bending vanishes for odd values of Θ. Thus, for every even value of Θ

,

$$< \Theta^2 > = l/Lp \qquad (4)$$

Thus, the average value of cosine between two segments separated with the length l is:

$$<\cos\Theta(l)> = \exp(-\lambda L) \qquad (5)$$

With $\lambda = 1/Lp$. Polymer molecules, at 2-D surface, such as mica tend to gain lowest energy conformation. Then, the mean square end -to-end distance is related with the cosine of angle Θ as:

$$<R^2>_{2D} = \int_0^L ds \int_0^L < \cos\big(\Theta(s) - \Theta(s')\big)\, ds' \qquad (6)$$

Using equation (5) in equation (6) and further calculation, an equation is obtained which relates the end-to end distance with persistent length in 3-D surface.

$$< R^2 >= (\frac{2}{\lambda^2}(\lambda L - 1 + \exp(-\lambda L)) \qquad (7)$$

The end-to-end distance is measured using FiberApp both experimentally as well as theoretically using the equation (7). The software calculates the minimum value of sum of square of difference between end-to-end distances obtained experimentally theoretically approaches as to the most probable value of persistent length $\lambda = 1/Lp$

CHAPTER III

RESULT AND DISCUSSION

3.1. Synopsis

This chapter includes the results obtained using AFM measurements in both imaging and QNM modes. The β-lg samples prepared at three different incubation times (24, 48, and 72 hours) at 80 ^{o}C. All samples were imaged in air at room temperature. Also, measurements were performed on several locations on the same sample and repeated at least three times using fresh protein solution each time. We were planning to perform more AFM measurements using QNM and AFM force spectroscopy but unfortunately during the last few months of the project the microscope stops working due to unstable power in M1 building. We hope that this issue will be fixed soon and this work need to be finished.

3.2. AFM Imaging at different Incubation time

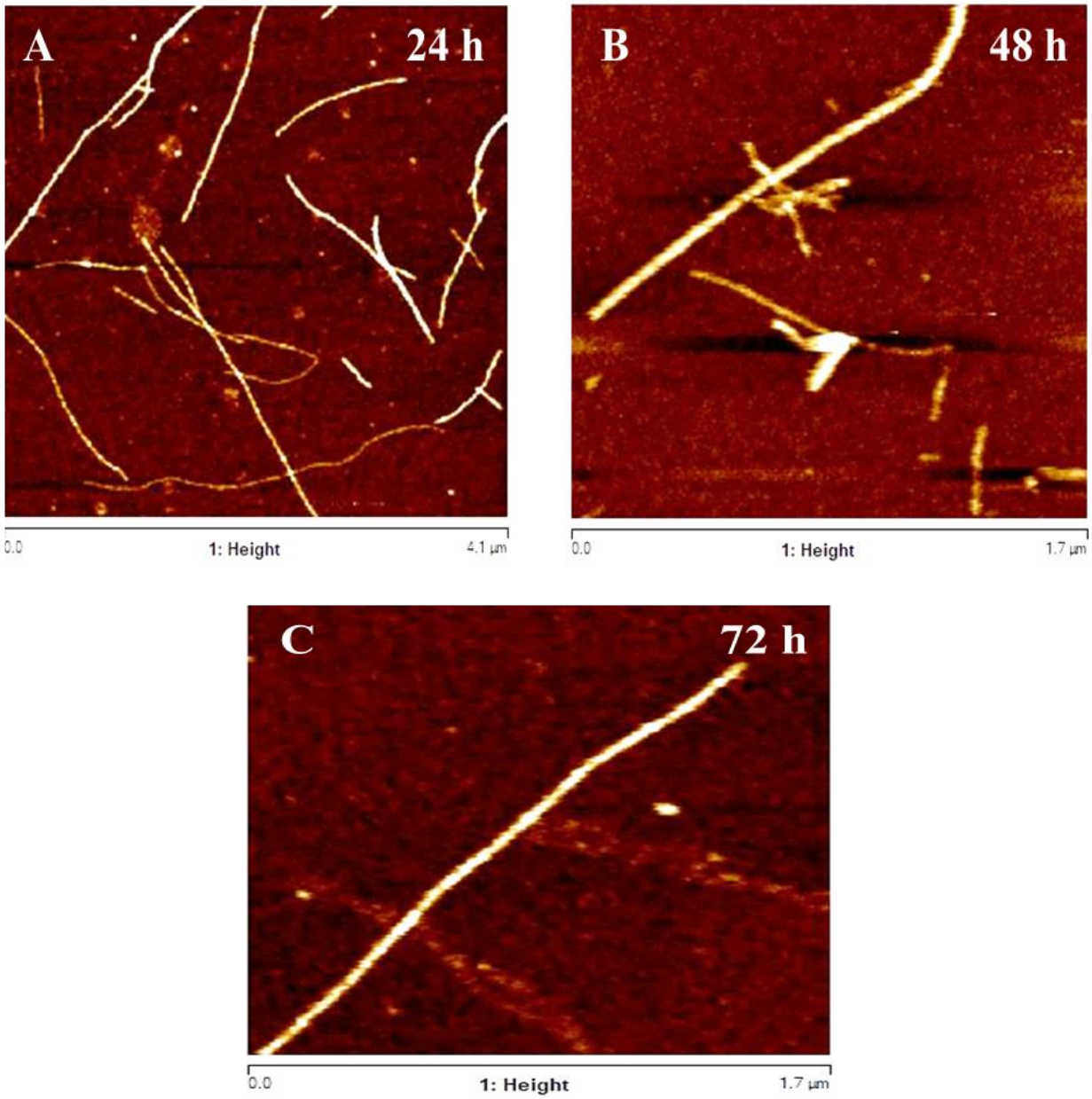

Figure10. AFM height images of β-lg fibers prepared at different incubation time. All other conditions were like all samples (heating temperature 80 ^{o}C, pH 2, and protein concentration 0.2% wt. A) fibers at 24 hours. B) fibers at 48 hours. C) fibers at 72 hours. All images were recorded in air using AFM contact mode.

The AFM height images shown in figure 10 are representative images of the fibrillary structures for the three incubation times. Single fibers can be imaged if very diluted solutions of the β-lg fibers are used. Overall, for the three incubation times fibers with various lengths and almost similar sizes were imaged at several locations of the sample. Hundreds of images were recorded and further analyzed using Nano scope analysis, WSXM, and FiperApp software. Statistical analysis of the structural and topological features of hundreds of β-lg fibers at each incubation times are performed and compared to each other to determine the topological effects of the incubation time on the fiber conformation. Thus, parameter such as, length, height, curvature, orientation, and mean-squared end-to-end distance can provide an unprecedented structural description of filamentous synthetic and biological objects.

3.2.1. Statistical analysis of the fiber height

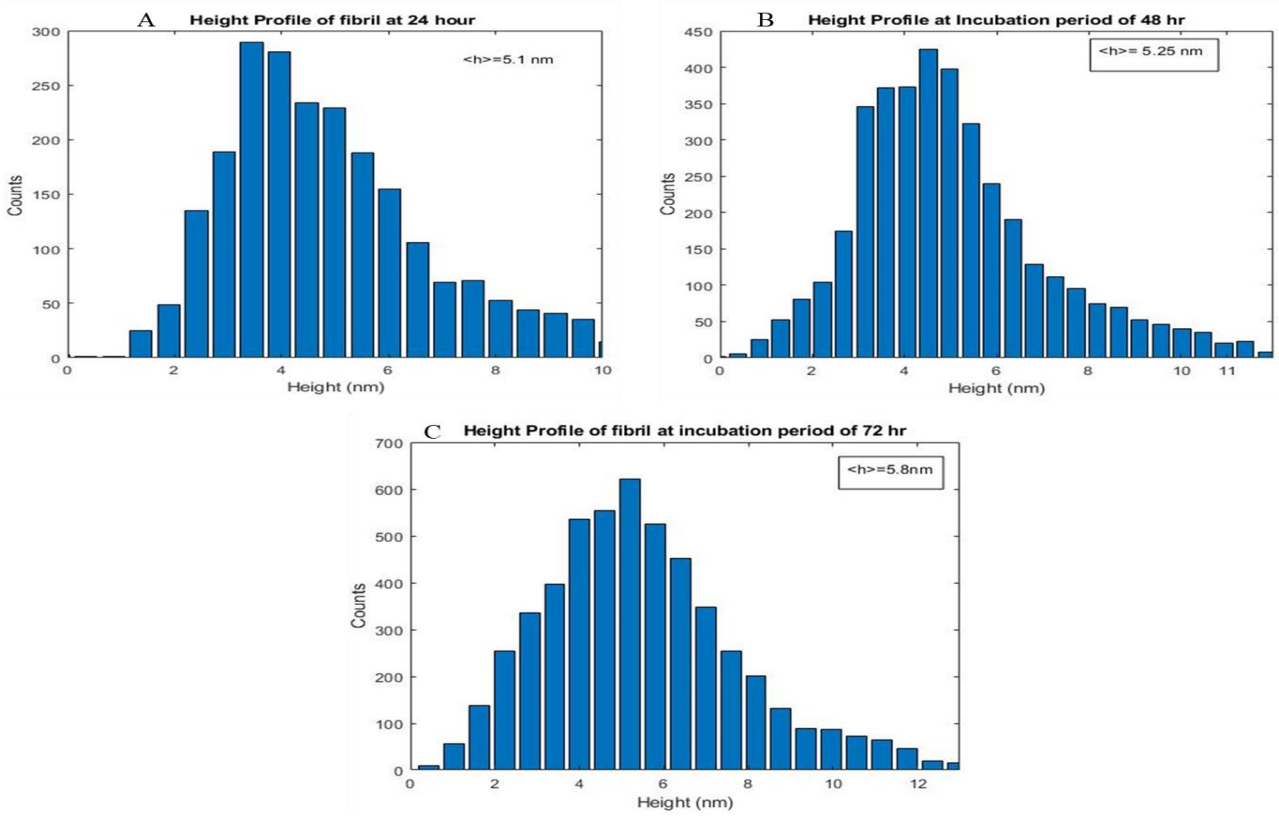

Figure 11. Statistical distributions of the heights of β-lg fibers for the three incubation times. The average height is 5.1 nm for 24 h, 5.25 nm for 48 h, and 5.8 nm for 72 h.

The statistical distributions of the heights of β-lg fibers shown in figure 11, were plotted using about 50 fibers for each incubation time. Only fibers with both ends clearly visible and homogeneous height along the whole fiber were selected. Also, no crossing or branched fibers were included in the distributions plotted using the FiberApp software. As shown in figure 11, no significant changes were observed in the fibers heights for the three temperatures with slight increase (~ 1nm) at 72 h compare to fibers prepared at 24 h.

3.3. Mechanical properties of β-lg fibers

3.3.1. Nanoscale ordering of β-lg fibers: Dimension of each monomer

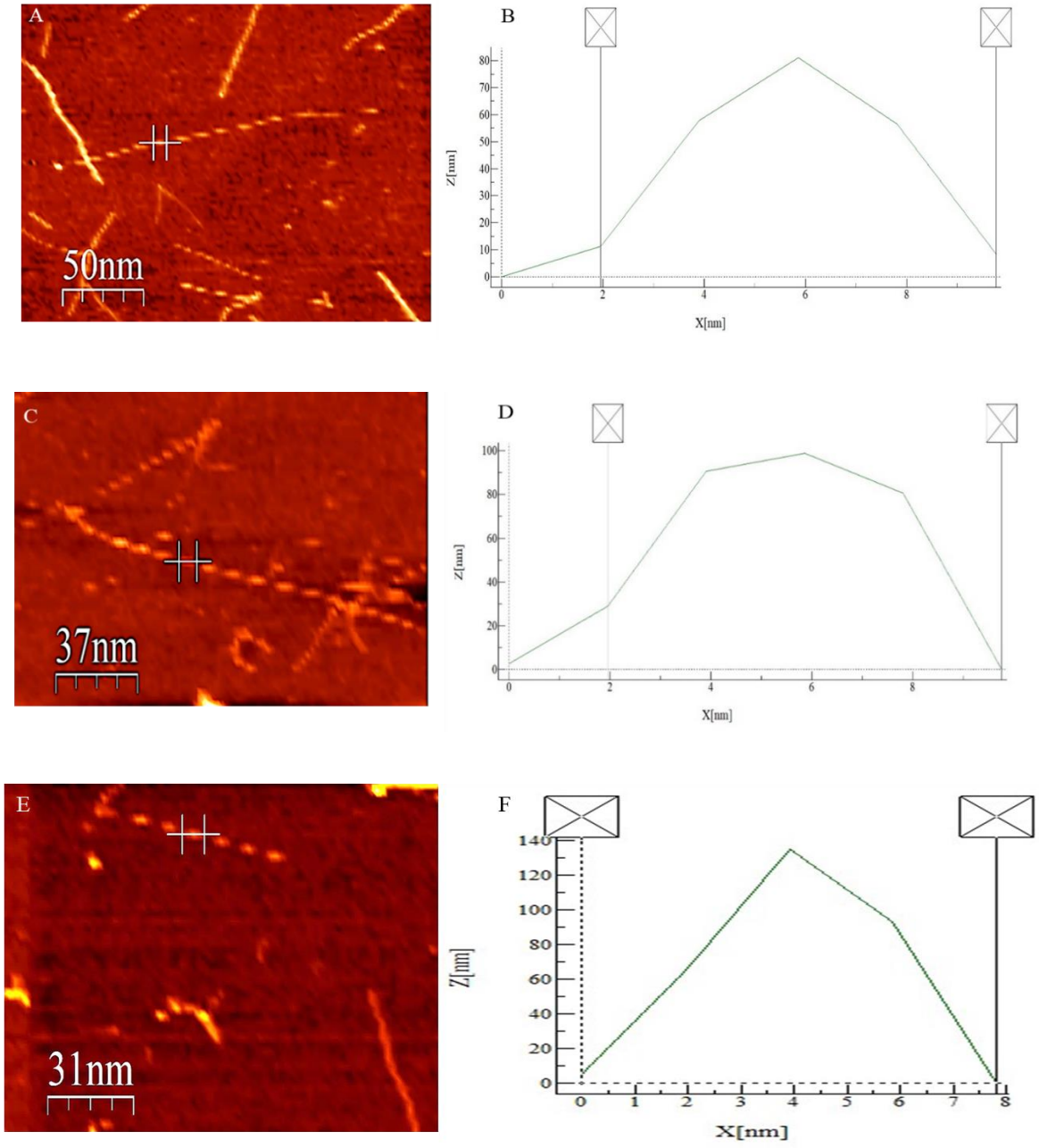

Figure 12. AFM-cross sections on single β-lg fibers showing the dimensions of single monomers for each incubation time. A, B) 24 h; C, D) 48 h; and E, F) 72 h.

Several AFM images were selected and zoomed until single monomers are clearly visualized. The dimensions of single monomers were then measured using AFM-cross section profiles using WSXM software as shown in figure 12. Like the heights of the fibers, the length of each monomer found not to change with the incubation times. For the three incubation times the length of single monomer was fix around 8 nm. Thus, the β-lg fibers can be described as single neckless with elliptical monomers with dimensions of ~ 5 × 8 nm and not affected with the incubation time of the fibrillation.

3.3.2. Peak force quantitative nanomechanical (QNM) measurements

As shown in figure 13, 14, and 15, the QNM mode was Also performed on all samples, to determine the mechanical properties of individual β-lg fiber for the three incubation times. The AFM NanoscopeAnalysis software was used to analyze the AFM images. The periodicity of the fibrils with the identical height, width, and with the same forms of polymorphism was almost identical and approximately 55 nm for all the incubation times (24 h, 48 h and 72 h).

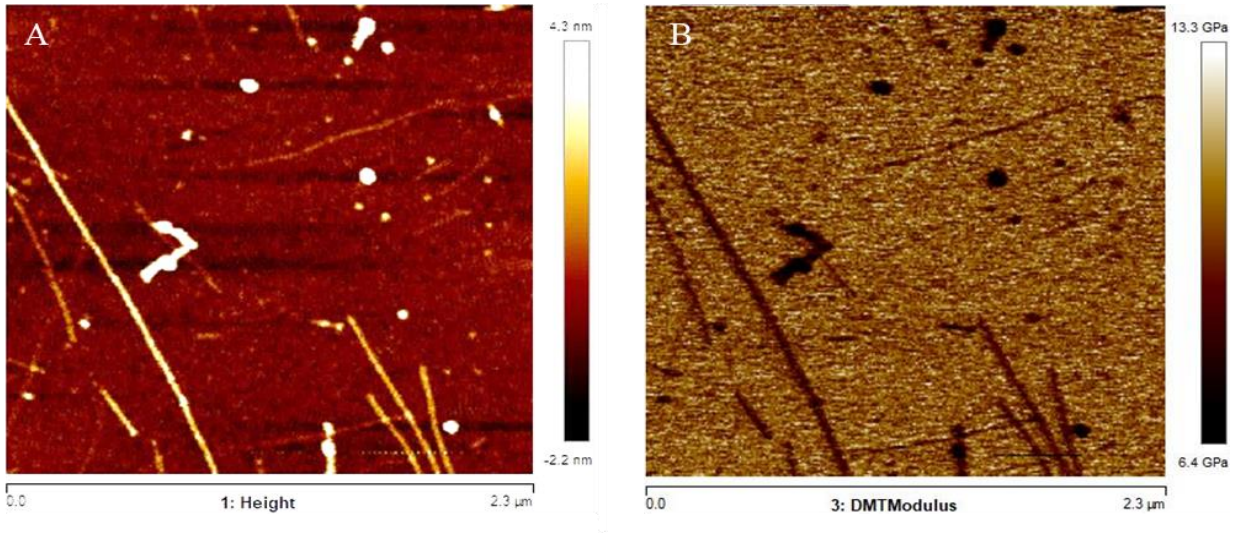

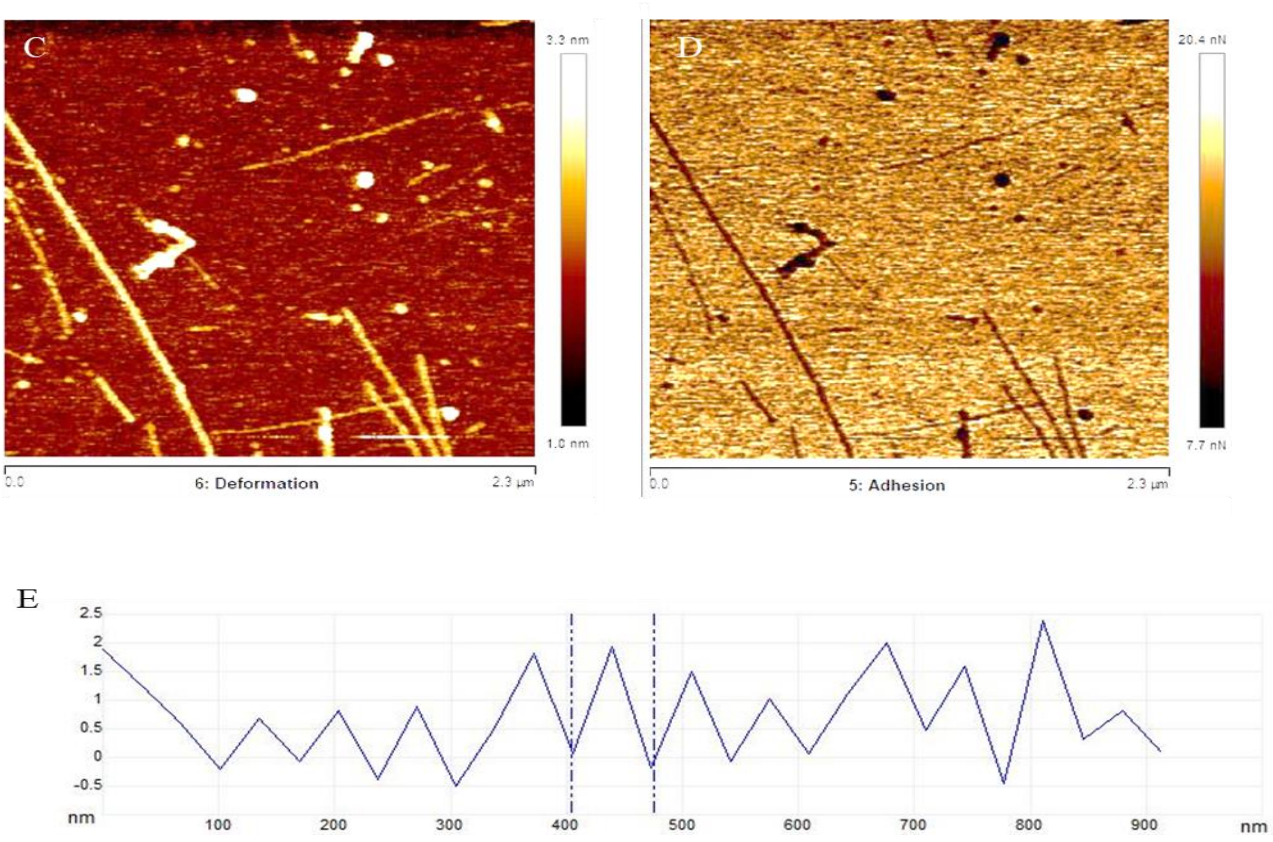

Figure 13. QNM measurements on the β-lg fibers grown at 24 h. A) An AFM height image showing several fibers on the mica surface. B) An AFM image of the Young's Modulus based on DMT model. C) An AFM image of the adhesion forces between the tip and the sample. D) An AFM image of the deformation of the sample due to the applied force by the tip. E) AFM cross-section on a single fiber showing the periodicity of ~ 55nm of the fiber.

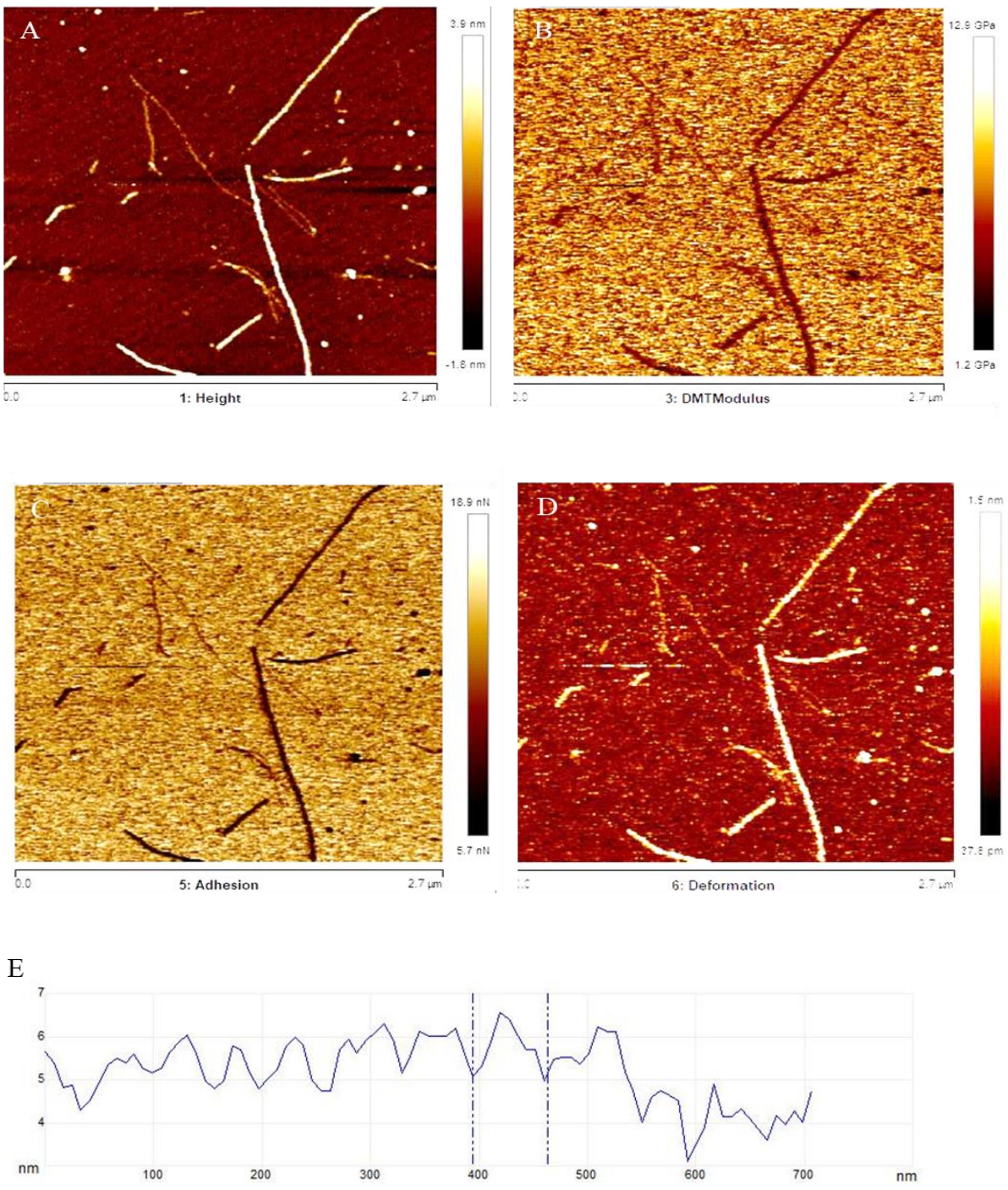

Figure 14. QNM measurements on the β-lg fibers grown at 48 h. A) An AFM height image showing several fibers on the mica surface. B) An AFM image of the Young's Modulus based on

DMT model. C) An AFM image of the adhesion forces between the tip and the sample. D) An AFM image of the deformation of the sample due to the applied force by the tip. E) AFM cross-section on a single fiber showing the periodicity ~ 58nm.

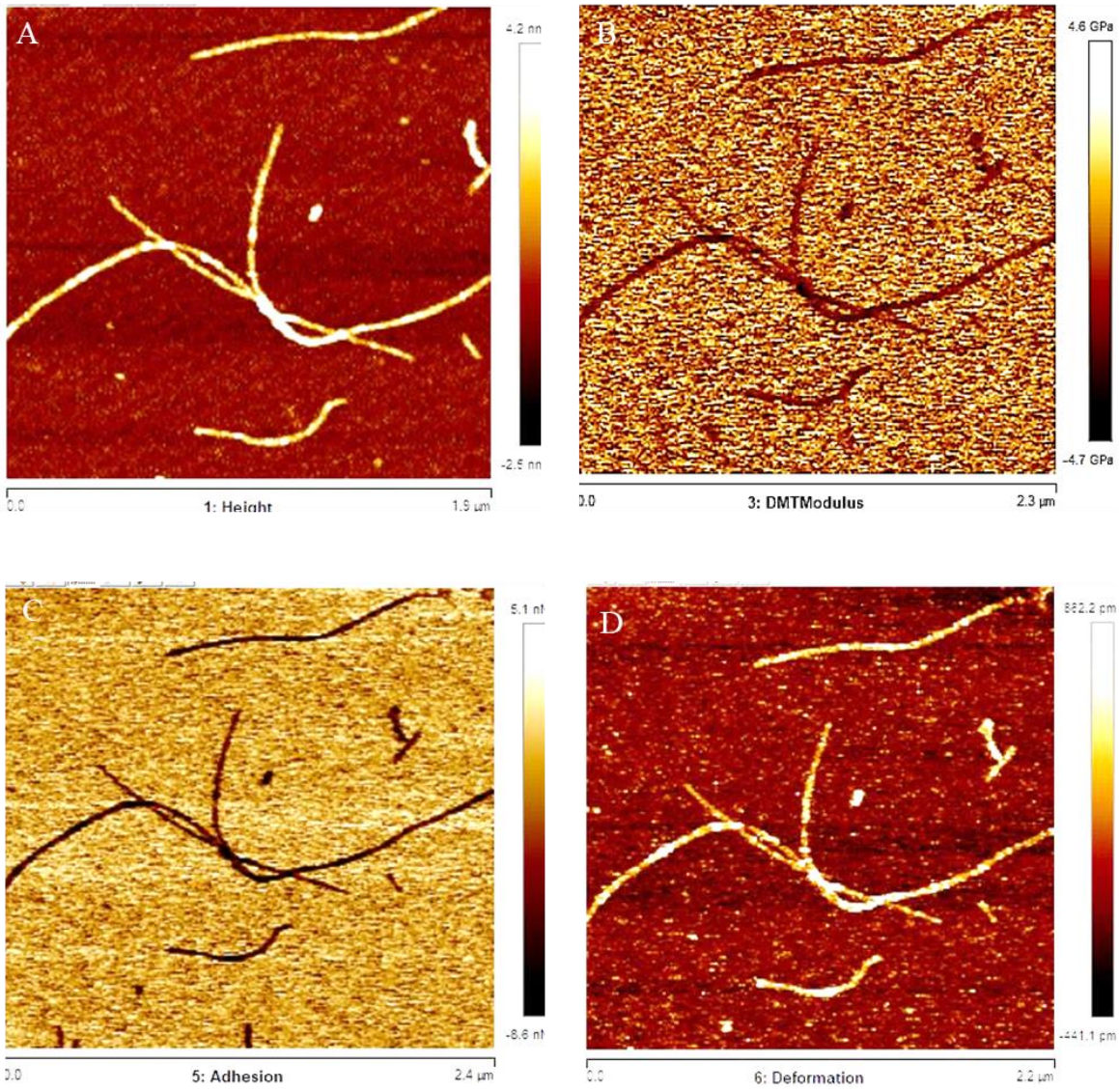

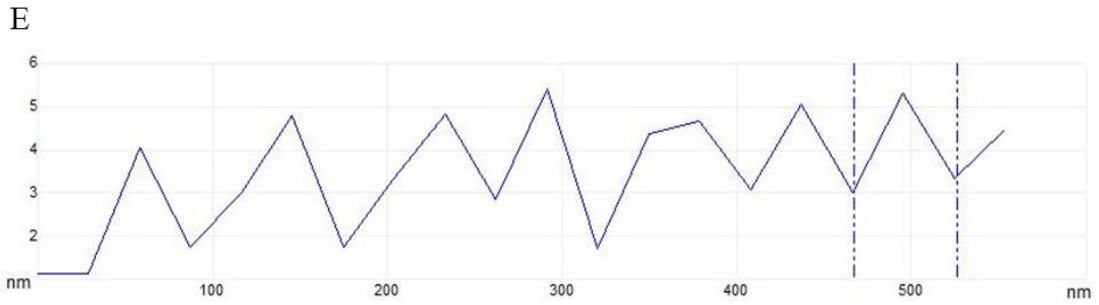

Figure 15. QNM measurements on the β-lg fibers grown at 72 h. A) An AFM height image showing several fibers on the mica surface. B) An AFM image of the Young's Modulus based on DMT model. C) An AFM image of the adhesion forces between the tip and the sample. D) An AFM image of the deformation of the sample due to the applied force by the tip. E) AFM cross-section on a single fiber showing the periodicity ~ 55nm.

3.3.3. Changes in mechanical properties during fibrillation process

AFM Nanoscope Analysis software was used to extract the Young's Modulus and deformation of β-lg fibers for the three incubation times. More than 30 fibers from 10 different AFM images were analyzed for each incubation period and statistical distributions of the moduli of elasticity were plotted and compared. A gradual decrease in modulus of elasticity of the β-lg

was observed upon increasing the incubation time period incubated from 24 h to 72 h.

A

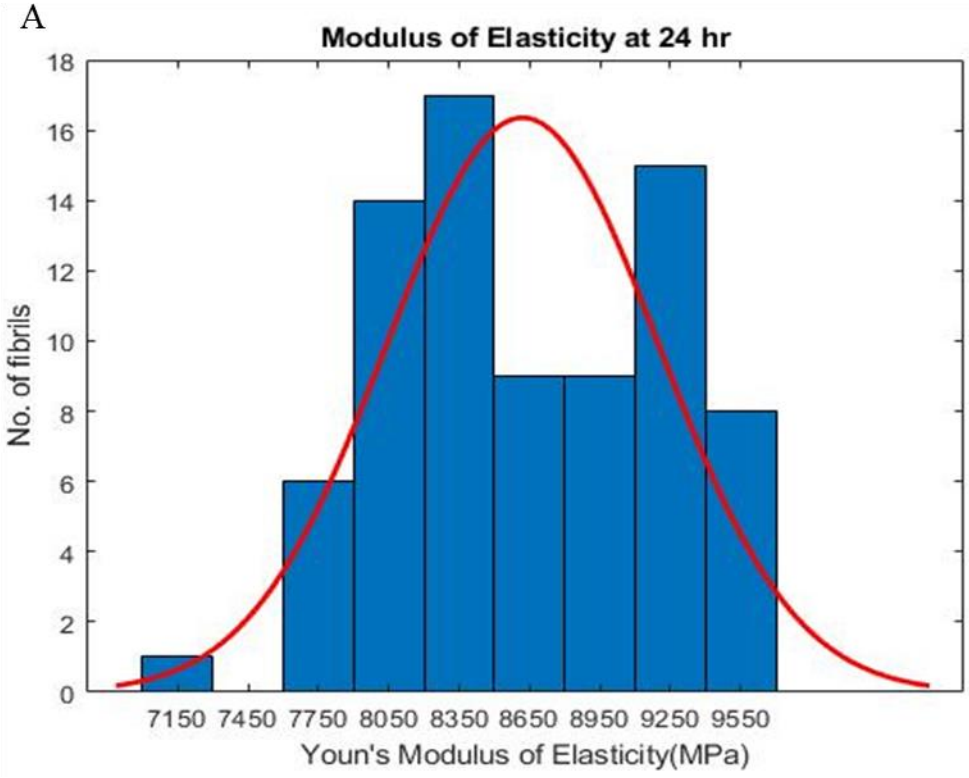

B

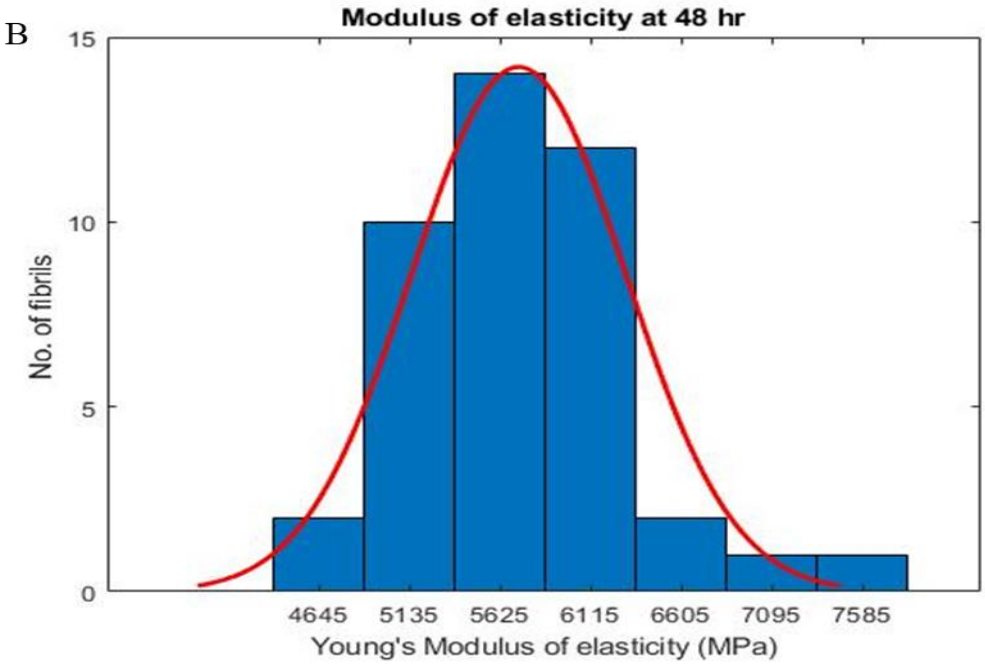

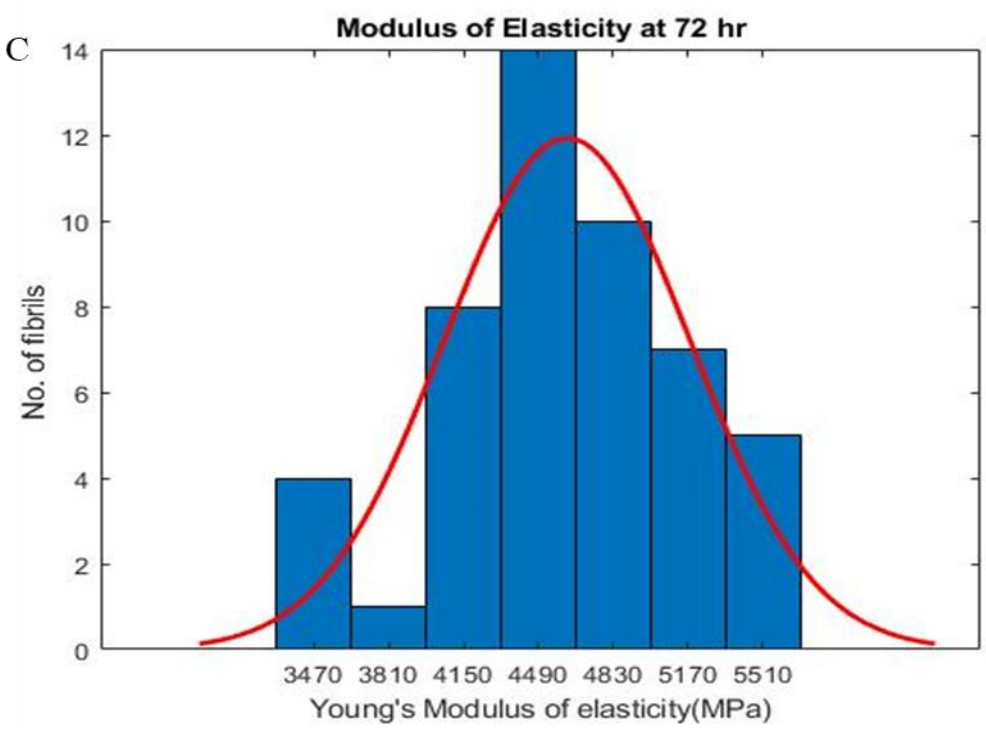

Figure 16. Statistical distributions of the Young's modulus calculated from the QNM measurements at each incubation time based on DMT model. A) 24 h, B) 48 h, and C) 72 h.

A

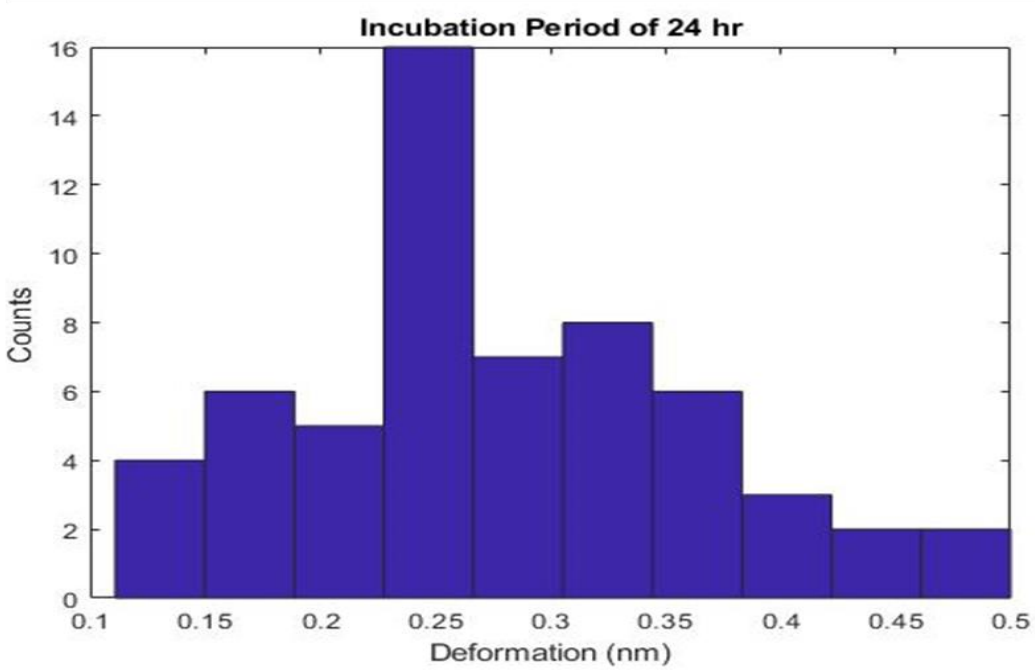
Incubation Period of 24 hr
Counts
Deformation (nm)
0
2
4
6
8
10
12
14
16
0.1
0.15
0.2
0.25
0.3
0.35
0.4
0.45
0.5

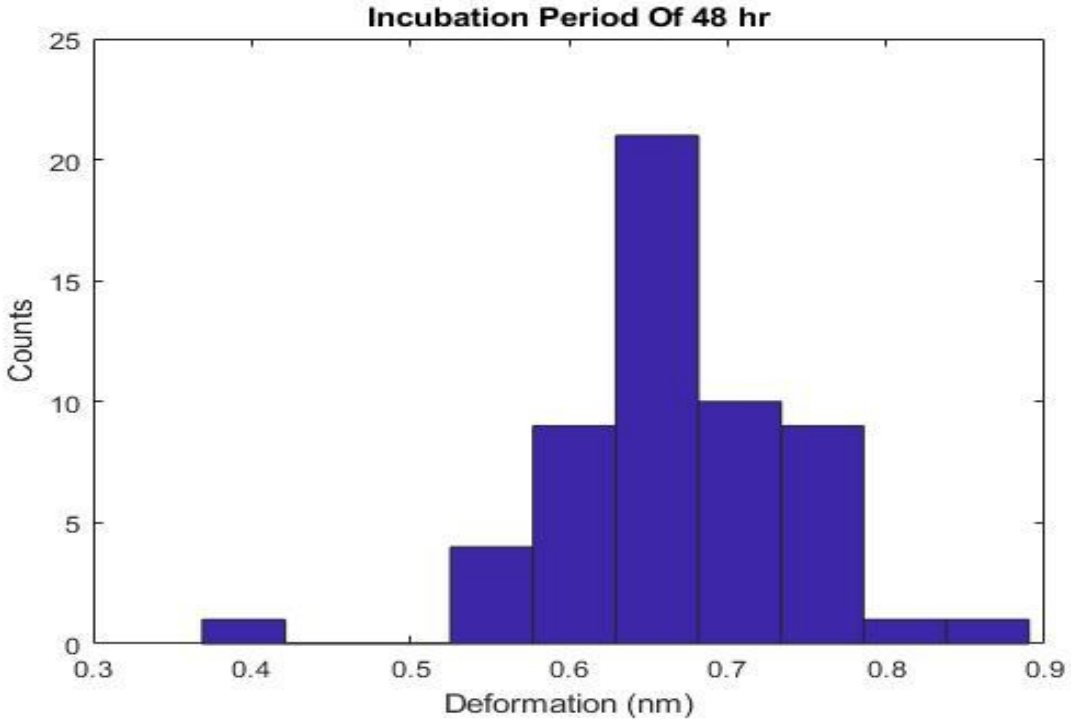
Incubation Period Of 48 hr
Counts
Deformation (nm)
0
5
10
15
20
25
0.3
0.4
0.5
0.6
0.7
0.8
0.9

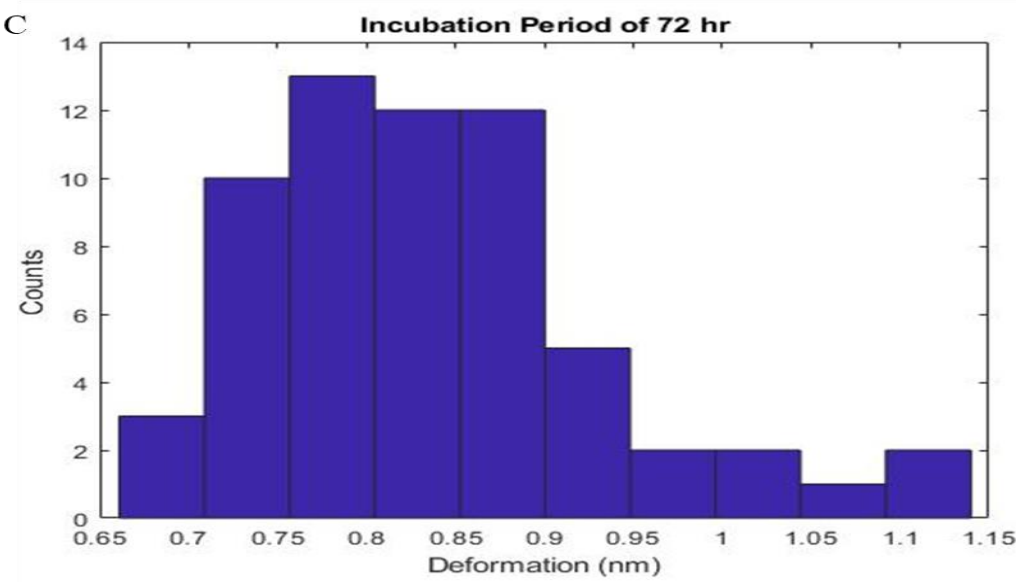

Figure 17. Statistical distributions of the deformation parameter calculated from the QNM measurements at each incubation time. A) 24 h, B) 48 h, and C) 72 h.

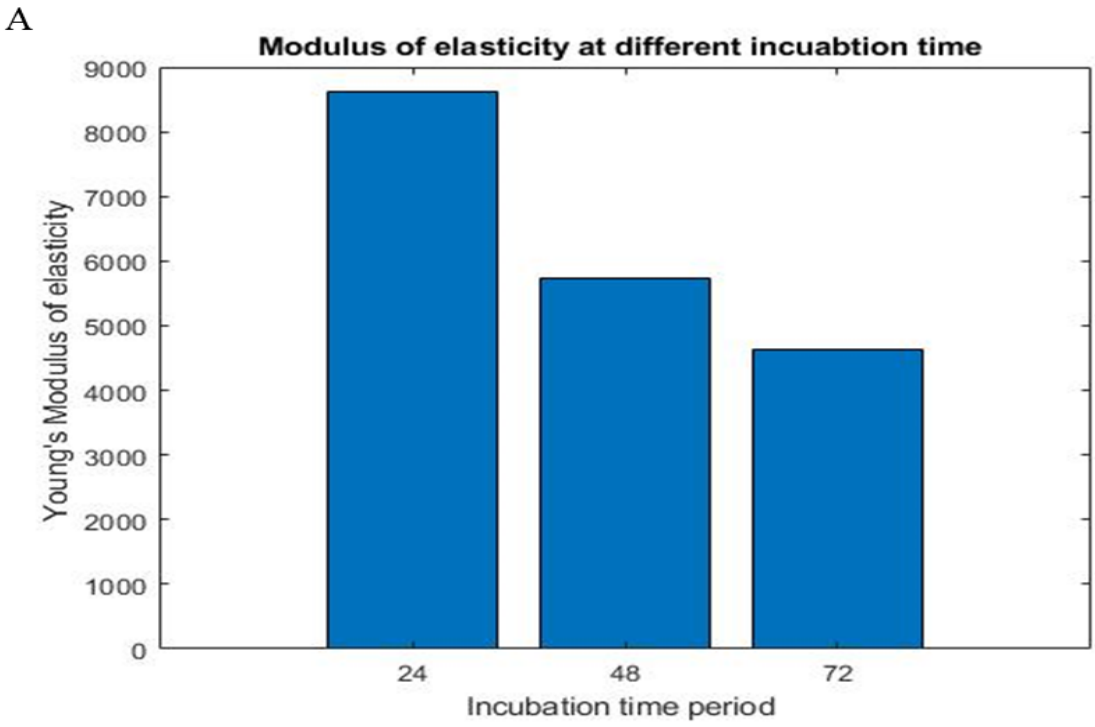

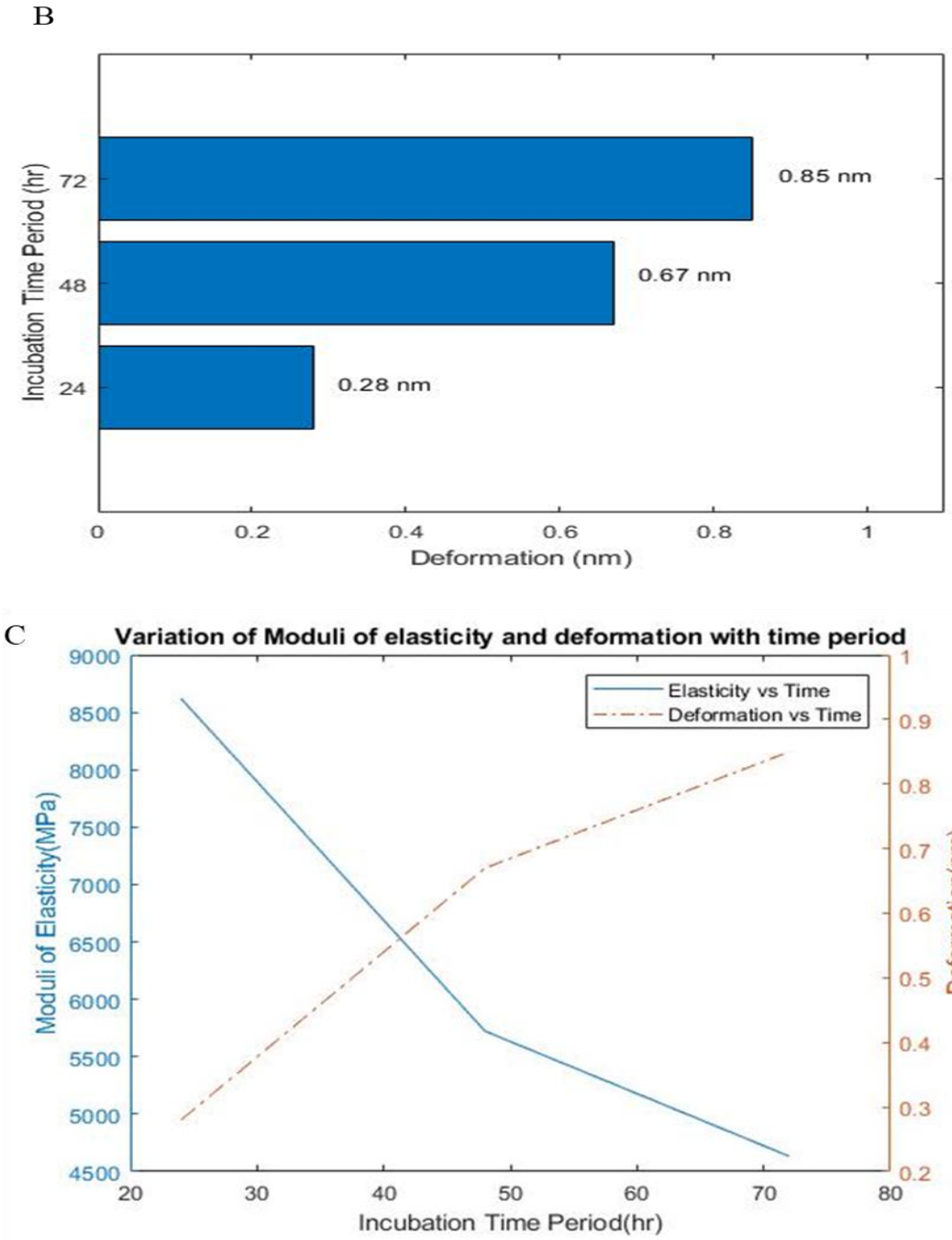

Figure 18. A-B) Histograms summarizing Young's Modulus and deformation measurements for the three-incubation time. A) The Young' modulus decreases with the incubation time. B) The

deformation was found to increase with time. C) Represents the relationship between moduli of elasticity and the deformation of β-lg fibers as the changes in incubation time. The solid line in cyan illustrates the variation of Young's Modulus of elasticity with the period of incubation and the yellow dotted line represents the change in deformation the fiber with incubation time.

As shown in figure 18A, the modulus of elasticity of β-lg fibers shows a significant decrease with the increase of incubation period. At 24 h, the average Young's Modulus was found to be about 8.6 GPa as shown in figure 16A, followed by modulus of elasticity of 5.7 GPa when the fibers were heated for 48 h (figure 16B), and the modulus of elasticity drops to 4.6 GPa when heated to 72 h (figure 16 C).

The histogram in figure 18B summarizes the deformation measurements for the three incubation periods. The β-lg deformation was higher at 72h compare to the other two times. As shown in figure 17 C, the average deformation of the fibers heated for 72 h is around 0.85 nm. This average decreases to 0.67 nm for fibers incubated for 48h, and to 0.28 nm for fibers heated for 24h.

This data shows that the gradual decrease in the modulus of elasticity, which is a decrease in the fiber's stiffness, is accompanied with a gradual increase in the fibers deformation with the increase in the incubation time.

3.3.4. Bending stiffness quantification: measurement of persistent length

Fiberapp was used to track the fibers and quantify the bending stiffness, persistent length of the fibers.

A

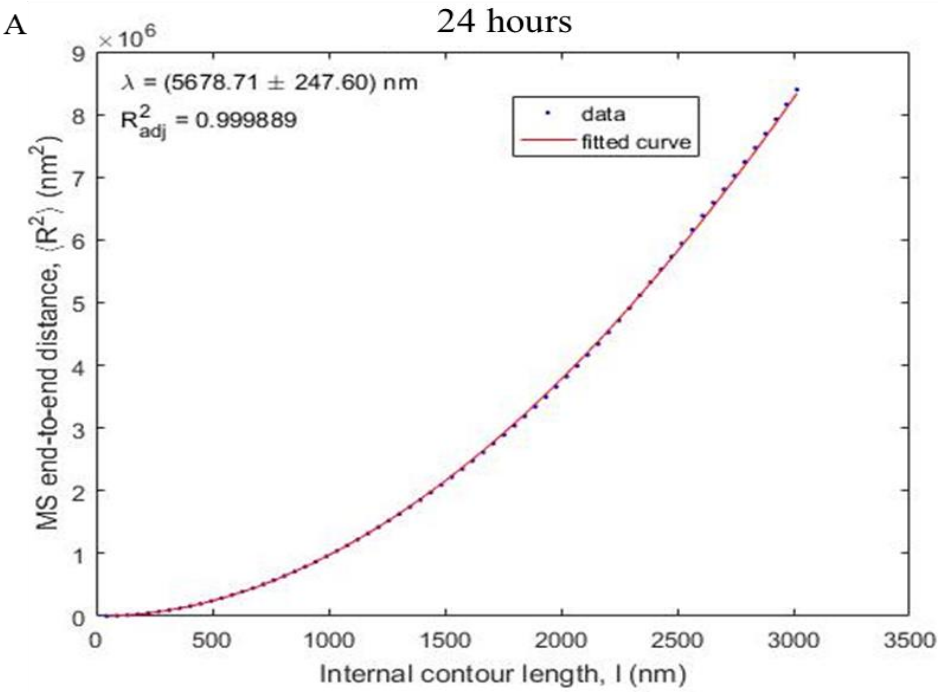
24 hours
×10^6
λ = (5678.71 ± 247.60) nm
R²adj = 0.999889
data
fitted curve
MS end-to-end distance, ⟨R²⟩ (nm²)
Internal contour length, l (nm)
0
1
2
3
4
5
6
7
8
9
0
500
1000
1500
2000
2500
3000
3500

B

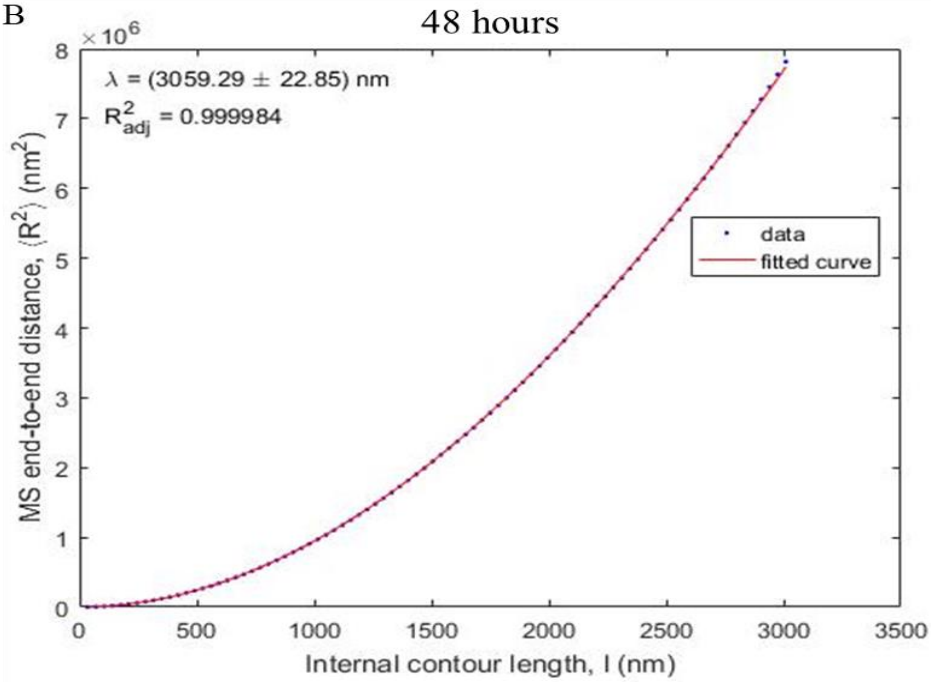
48 hours
×10^6
λ = (3059.29 ± 22.85) nm
R²adj = 0.999984
data
fitted curve
MS end-to-end distance, ⟨R²⟩ (nm²)
Internal contour length, l (nm)
0
1
2
3
4
5
6
7
8
0
500
1000
1500
2000
2500
3000
3500

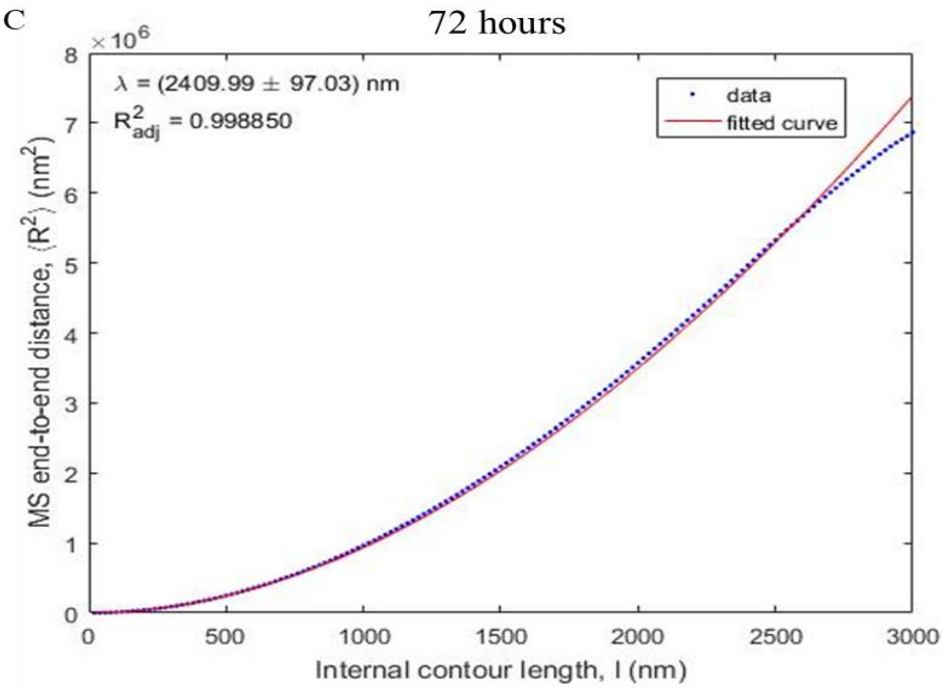

Figure 19. Graphs of mean square-end-to-end versus counter length of β-lg fibers at the three incubation times. The dotted lines represent the experimental calculated values of mean-square-end-to-end distance of the fibers with respect to their counter lengths (using FiberApp software). The red line is the fitting of the experimental data. A) The persistent length for fibers grown of 24 hours was estimated ~ 5.67 μm. B) for fibers heated for 48 hours the persistent length was ~ 3.05 μm. C) shows the persistent length of 2.4 μm for the fibers incubated for 72 hours. The persistence lengths of the β-lg were lower at higher incubation time.

3.3.5. Identical Moduli of elasticity of different polymorphic forms of amyloid fibrils

Three different polymorphic forms of the β-lg fibrils, incubated for 24 h, were identified with careful investigation using Nasoscope Analysis software. The three different polymorphic

forms are: twisted ribbon, helical ribbon, nanotube like structure. Only the fibers with identical morphology (height,width) were selected for the study.

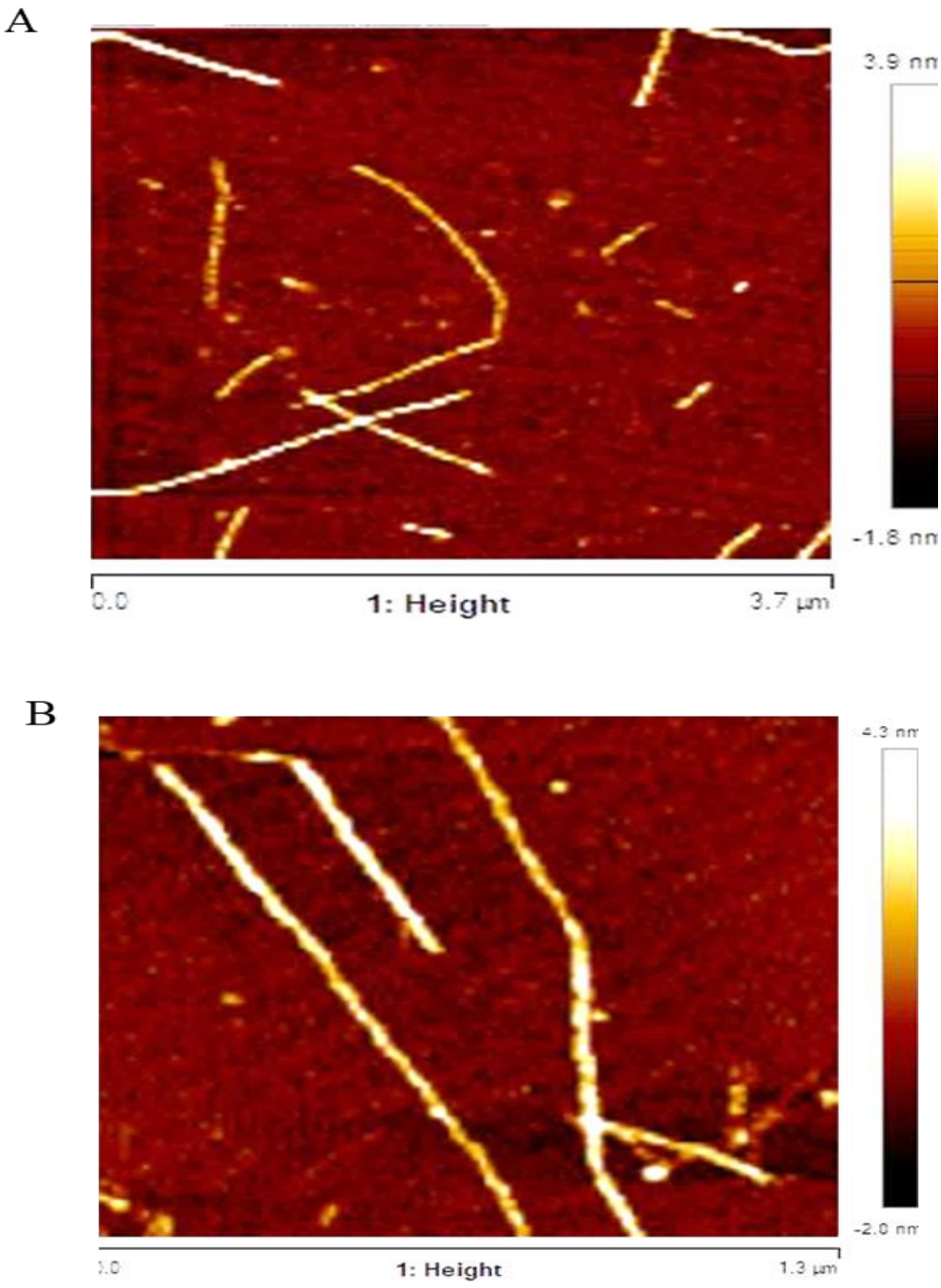

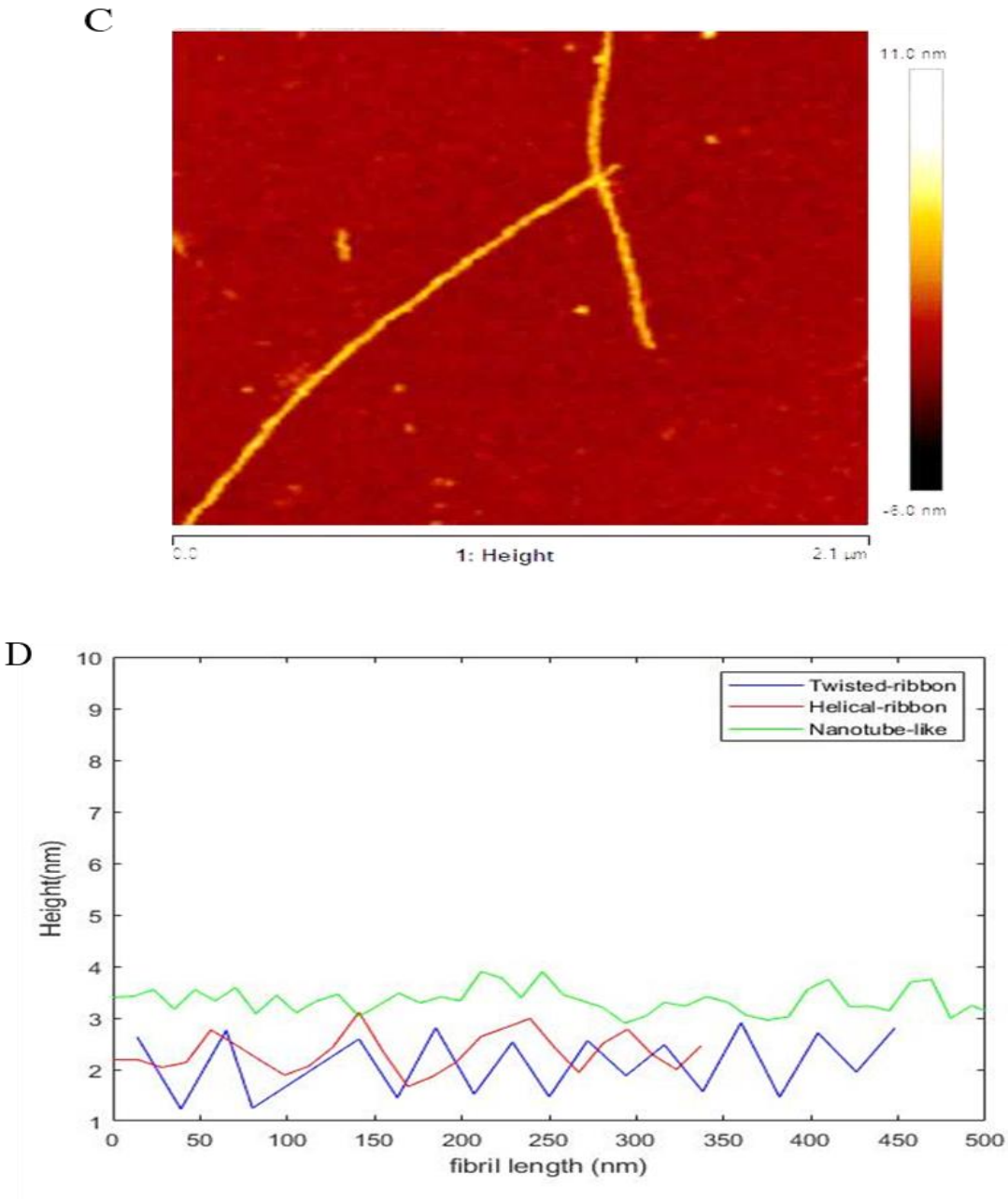

Figure 20. A-C) AFM height images showing three different polymorphic forms of β-lg fibrils observed in fibers incubated for 24h. A) Twisted ribbon, B) Helical Ribbon, and C) Nanotube-like structure. D) AFM cross-sections, taken on single fibers on each AFM image, showing the periodicity of the twisted ribbon (blue), Helical ribbon (red) and Nanotube-like structure (green).

The young's modulus of elasticity of twisted ribbon was found to be 8.25 GPa, that of helical ribbon was calculated to be 8.47 GPa and that of nanotube-like structure was found to be 8.5 GPa. There is slight difference in the value of moduli of elasticity. Moduli of elasticity does not seem to vary upon different polymorphic forms of the fibrils.

3.4 Discussion

The β-lg fibrillation process required a long incubation period of about one day with protein concentration of 2 % wt. and low pH level (2-3). Also, the fibrils solution needs to be diluted enough (0.5% wt.) to image isolated individual fibers. Parameters like periodicity, height and dimension of the fibers were studied to investigate whether the different incubation period affects the morphological characteristics or not. Also, a part of our study was to investigate whether the increase in incubation period affects the dimension of the monomer or not. The AFM images with distinguishable fibers were analyzed and zoomed using the WSXM software, to observe the individual monomer. Our data showed that regardless of the incubation time, the monomeric unit of β-lg fibers, prepared under similar conditions, has an elliptical shape with dimension of 8×5 nm.

Equal number of fibers were chosen for tracking procedure using FiberApp. 50 fibers were selected for each of the incubation period, whose height and both ends were clearly visible. Most of the chosen fibers were isolated however, some of them were crossed with each other but were clearly distinguishable. Fibers were tracked and height profile was calculated. Average height of 50 fibrils for each of the incubated period was determined to be about (5.1nm for 24h, 5.25 nm for 48h, and 5.8 nm for 72 h). The slight variation in these values might be due to the cross linkage

between the fibril and the ups and down surface of the substrate. Also, the AFM force used during imaging in air sometimes increases (due to capillarity) during the image recording process, which affects the height of the imaged objects. However, thicker fibrils of heights well beyond 6 nm were also occasionally observed. Other valuable structural details, such as fibril splitting or fibril thinning, were also observed by our AFM measurements. The height of the thicker parts was found to be almost twice the height of the thinner parts. Future investigations are needed to determine the physical mechanisms behind these structures.

In addition, further structural detail that could be observed and resolved was a periodic height fluctuation along the contour of the fibrils. The periodicity of the fibrillary structure was almost identical for the three incubation periods (~55 nm). The presence of periodic fluctuations in height along the contour length of amyloid fibrils is controversial and a matter of debate in the literature. Gosal and colleagues, who studied fine filaments, were unable to observe any periodic structure in β-lactoglobulin fibrils (Gosal et al., 2002, 2004). In the same systems, however, Arnaudov and colleagues observed a periodic structure with a period of ~26 nm (Arnaudov et al., 2003). A detailed study on β-lactoglobulin amyloid fibrils, by Adamcik et al.(Adamcik et al., 2010), demonstrated the presence of a periodic structure with different periods for different heights. Thus, the periodicity was found to increase linearly with the height of the fibrils with four different periods (35, 75, 100 and 135 nm), corresponding to fibril maximum heights of 4, 6, 8 and 10 nm, respectively.

To further investigate the relationship between the structural and mechanical properties of the β-lg fibers, we analyzed the changes of persistence length with incubation time. The persistence

length lp was determined directly from the AFM images by means of the bond correlation function for semi-flexible polymers in a two-dimensional conformation. The persistent length is a physical parameter for quantifying the mechanical stiffness of a polymer such as protein and DNA and was measured using the FiberApp, which is based on worm-like chain model. The AFM images were first flattened and tracking procedure was applied. About 50 good fibers were chosen and the same processing length was applied for each of the incubated period. The mean-square end to end distance was calculated using both theoretical as well as experimental approach with respect to the given counter length. Equation 7 was used to calculate the theoretical mean-square-distance for different values of Lp. The experimental value was obtained upon tracking by the software. The software detects the specific value of persistent length, Lp for which square of difference between theoretical value and experimental value of Lp is minimum which is the most probable value of persistent length. The persistent length of fibers incubated for 24 h was measured to be ~5.67μm, that of 48 h was measured to be ~3.05 μm and for incubation period of 72 hr, it was found to be ~2.4 μm. This data shows that the stiffness of β-lg fibers incubated for three days (72 h) was decreased more than half compare to the stiffness of the fibers heated for 24 h. It can also be stated that longer the fibril is subjected to thermal fluctuation, more it will be flexible. The mechanism behind the heat effect on amyloid fiber mechanics is not yet established. However, we believe that the monomer of heated fibers, for long period of time, are subject to internal relaxation with changes in protein conformations.

It was also observed in our study that fibrils with different height from ~2nm to ~6nm were observed. The thinner fibril with height of 2 nm might be the protofibril and the thicker fibril with height 6 nm might be the mature fibril composed of multiple protofibrils. The Young's modulus

of thin fibril was observed to have higher value than that of the thicker fibrils. Moreover, some of the globular forms of the β-lg were also seen with lower values of modulus of elasticity than the fibrils.

In addition, the average Young's Modulus of elasticity was found in Giga Pascal range which is comparable to result obtained from previous study. High value of the young's modulus of the fiber indicate the tight, densely packed core. The modulus of elasticity in such a high range of GPa corroborates the presence of β-sheets folded protein containing strong hydrogen bonding. Protein-based amyloid fibrils can show a great variety of polymorphic structures within the same protein precursor, although the origins of these structural homologues remain poorly understood(Usov et al., 2013) In the present study, three different polymorphic forms were identified for fibers incubated for 24; twisted ribbon, helical ribbon and nanotube-line structure. Similar values of moduli of elasticity (8.25GPa for 24 h, 8.47 GPa for 48 h and 8.5 for 72h) were measured for the three different forms, which indicates that the intrinsic structure remains the same for the fibril with the different morphological forms. It can also be inferred that for a same thermal energy, the modulus of elasticity predicted to remain same.

CHAPTER IV

CONCLUSION AND FUTURE PRESPECTIVES

A key reason for the longstanding and widespread interest in the biophysical and biochemistry studies of amyloids fibrillation is the strict link with several human illnesses and neurodegenerative diseases. Despite its fundamental role in biological function and malfunction, the mechanism of protein aggregation and the fundamental origins of the connection between the aggregation process and cellular toxicity have remained challenging to elucidate in molecular detail. Strong evidence intimately correlated the physical and structural properties of intermediate and final forms of amyloids to the biochemistry of neurodegeneration. However, the molecular origins of the process of neurodegeneration and its connection with amyloid formation remain unclear and there is no cure to the related diseases. Therefore, the unraveling of the mechanisms of amyloid formation and polymorphism, as well as the mechanical and structural properties of the products of their aggregation is fundamental to understand their stability, toxicity and mechanism of clearance in the body. This is central in order to design new therapeutic strategies to the diseases problem. Furthermore, it has been recently found that it exists an always-bigger class of functional amyloids occurring naturally in several disease-unrelated biological processes and that many artificial peptides can form amyloid-like structures in-vitro. For this reason, in order to appreciate the full potential of amyloid fibrils also as biomaterials for future biomedical and nanotechnology applications, it is important to measure and quantify the structural and

mechanical properties of amyloid fibrils and understand how they emerge from the fibrillization process. In the frame of this thesis, we have been able to bring new insight into the nanoscale investigation of the effects of incubation temperature on the mechanical properties of amyloid fibers and on the structural properties of the products of the aggregation. Together with conventional AFM imaging, we reported the successful application of nanomechanical mapping (PF-QNM) to inquire the nature of the notable intrinsic stiffness of amyloid fibers. In summary, by performing a statistical analysis on single-molecule AFM and PF-QNM images, we were able to demonstrate that the overall structure of β-lg fibers, grown at pH 2 and 80 ^{o}C, was not affected during long incubation periods. However, the mechanical properties of these fibers were very sensitive to the incubation time. Fibers spending more time at 80 ^{o}C were found to be more flexible and deformable. We attributed the high values of elasticity modulus (giga-pascal range), of these fibers to the presence of cross-β sheet structure. Thus, we concluded that amyloid state is thermodynamically much more stable than the native and globular form of protein. We assume that incubation period has been observed to have significant effects on the mechanical properties, such as young's modulus, deformation of the fibril. Increase in incubation period makes the protein expose to heating environment for longer time, which vibrates the molecule continuously. We hypothesize that the interlayer distance between beta-sheet increases reducing the backbone Hydrogen bonding with more heat exposure which makes the fibril mechanically unstable and less stiff. Thus, the decrease in mechanical stiffness on increasing incubation period might be due to decrease in hydrogen bonding density in fibril structure.

Due the short time of this study and the problems encountered with our microscope, we were unable to investigate other structural and mechanical properties of these amyloid fibers. We hope that as future work our group will accomplish the following:

- Using AFM force spectroscopy to investigate the conformational changes in protein aggregates due to the incubation time.
- The dynamics of the fiber formation by performing in-situ high resolution imaging of the fibers formation in real time using heated AFM microscopy
- Comparing β-lg fibers with other protein fibers involved in neurodegenerative diseases

REFERENCES

Adamcik, J., Jung, J. M., Flakowski, J., De Los Rios, P., Dietler, G., & Mezzenga, R. (2010). Understanding amyloid aggregation by statistical analysis of atomic force microscopy Images.NatureNanotechnology, 5(6), 423–428. https://doi.org/10.1038/nnano.2010.59

Adamcik, J., & Mezzenga, R. (2011). Adjustable twisting periodic pitch of amyloid fibrils. Soft Matter, 7(11), 5437–5443. https://doi.org/10.1039/c1sm05382e

Adamcik, J., & Mezzenga, R. (2012). Proteins fibrils from a polymer physics perspective. Macromolecules, 45(3), 1137–1150. https://doi.org/10.1021/ma202157h

Arnaudov, L. N., de Vries, R., Ippel, H., & van Mierlo, C. P. M. (2003). Multiple steps during the formation of β-lactoglobulin fibrils. Biomacromolecules, 4(6), 1614–1622. https://doi.org/10.1021/bm034096b

Ban, T., Yamaguchi, K., & Goto, Y. (2006). Direct observation of amyloid fibril growth, propagation, and adaptation. Accounts of Chemical Research, 39(9), 663–670. https://doi.org/10.1021/ar050074l

Biancalana, M., & Koide, S. (2010). Molecular mechanism of Thioflavin-T binding to amyloid fibrils. Biochimica et Biophysica Acta - Proteins and Proteomics, 1804(7), 1405–1412. https://doi.org/10.1016/j.bbapap.2010.04.00

Cao, Y., & Mezzenga, R. (2019). Food protein amyloid fibrils: Origin, structure, formation,

characterization, applications and health implications. Advances in Colloid and Interface Science, 269, 334–356. https://doi.org/10.1016/j.cis.2019.05.002

Cappella, B., & Dietler, G. (1999). Force-distance curves by atomic force microscopy. Surface Science Reports, 34(1–3), 1–3. https://doi.org/10.1016/S0167-5729(99)00003-5

Claesson, P. M., Dobryden, I., Li, G., He, Y., Huang, H., Thorén, P. A., & Haviland, D. B. (2017). From force curves to surface nanomechanical properties. Physical Chemistry Chemical Physics, 19(35), 23642–23657. https://doi.org/10.1039/c7cp02612a

de Jongh, H. H. J., & Broerse, K. (2012). Application Potential of Food Protein Modification. Advances in Chemical Engineering. https://doi.org/10.5772/32114

DiFiglia, M., Sapp, E., Chase, K. O., Davies, S. W., Bates, G. P., Vonsattel, J. P., & Aronin, N. (1997). Aggregation of huntingtin in neuronal intranuclear inclusions and dystrophic neurites in brain. Science, 277(5334), 1990–1993. https://doi.org/10.1126/science.277.5334.1990

Flower, D. R., North, A. C. T., & Sansom, C. E. (2000). The lipocalin protein family: Structural and sequence overview. Biochimica et Biophysica Acta - Protein Structure and Molecular Enzymology, 1482(1–2), 9–24. https://doi.org/10.1016/S0167-4838(00)00148-5

Glenner, G. G., & Wong, C. W. (1984). Alzheimer's disease: Initial report of the purification and characterization of a novel cerebrovascular amyloid protein. Biochemical and Biophysical Research Communications, 120(3), 885–890. https://doi.org/10.1016/S0006-291X(84)80190-4

Gosal, W. S., Clark, A. H., Pudney, P. D. A., & Ross-Murphy, S. B. (2002). Novel amyloid fibrillar networks derived from a globular protein: β-lactoglobulin. Langmuir, 18(19), 7174–7181. https://doi.org/10.1021/la025531a

Gosal, W. S., Clark, A. H., & Ross-Murphy, S. B. (2004). Fibrillar β-lactoglobulin gels: Part 1. Fibril formation and structure. Biomacromolecules, 5(6), 2408–2419. 2. https://doi.org/10.1021/bm049659d

Gosal, W. S., Morten, I. J., Hewitt, E. W., Smith, D. A., Thomson, N. H., & Radford, S. E. (2005). Competing pathways determine fibril morphology in the self-assembly of β2-microglobulin into amyloid. Journal of Molecular Biology, 351(4), 850–864. https://doi.org/10.1016/j.jmb.2005.06.040

Ha, E., & Zemel, M. B. (2003). Functional properties of whey, whey components, and essential amino acids: Mechanisms underlying health benefits for active people (Review). Journal of Nutritional Biochemistry, 14(5), 251–258. https://doi.org/10.1016/S0955-2863(03)00030-5

Hua, Y., & Ph, D. (2014). PeakForce-QNM Advanced Applications Training 2014. Notes.

Kalapothakis, J. M. D., Morris, R. J., Szavits-Nossan, J., Eden, K., Covill, S., Tabor, S., Gillam, J., Barran, P. E., Allen, R. J., & MacPhee, C. E. (2015). A kinetic study of ovalbumin fibril formation: The importance of fragmentation and end-joining. Biophysical Journal, 108(9), 2300–2311. https://doi.org/10.1016/j.bpj.2015.03.021

Lambrecht, M. A., Jansens, K. J. A., Rombouts, I., Brijs, K., Rousseau, F., Schymkowitz, J., & Delcour, J. A. (2019). Conditions Governing Food Protein Amyloid Fibril Formation. Part II: Milk and Legume Proteins. Comprehensive Reviews in Food Science and Food Safety, 18, 1277–1291. https://doi.org/10.1111/1541-4337.12465

Li, C., & Mezzenga, R. (2012). Functionalization of multiwalled carbon nanotubes and their pH-responsive hydrogels with amyloid fibrils. Langmuir, 28(27), 10142–10146. https://doi.org/10.1021/la301541d

Maji, S. K., Perrin, M. H., Sawaya, M. R., Jessberger, S., Vadodaria, K., Rissman, R. A., Singru, P. S., Nilsson, K. P. R., Simon, R., Schubert, D., Eisenberg, D., Rivier, J., Sawchenko, P., Vale, W., & Riek, R. (2009). Functional amyloids as natural storage of peptide hormones in pituitary secretory granules. Science, 325(5938), 328–332. https://doi.org/10.1126/science.1173155

MC Bewley. (1997). Bovine beta-lactoglobulin and its variants: a three-dimensional structural perspective. International Dairy Federation. http://pascal-francis.inist.fr/vibad/index.php?action=getRecordDetail&idt=2431662

Micsonai, A., Wien, F., Kernya, L., Lee, Y. H., Goto, Y., Réfrégiers, M., & Kardos, J. (2015). Accurate secondary structure prediction and fold recognition for circular dichroism spectroscopy. Proceedings of the National Academy of Sciences of the United States of America, 112(24), E3095–E3103. https://doi.org/10.1073/pnas.1500851112

Mostaert, A. S., Higgins, M. J., Fukuma, T., Rindi, F., & Jarvis, S. P. (2006). Nanoscale mechanical characterisation of amyloid fibrils discovered in a natural adhesive. Journal of Biological Physics, 32(5), 393–401. https://doi.org/10.1007/s10867-006-9023-y

Ni, M., Zhuo, S., Iliescu, C., So, P. T. C., Mehta, J. S., Yu, H., & Hauser, C. A. E. (2019). Self-assembling amyloid-like peptides as exogenous second harmonic probes for bioimaging applications. Journal of Biophotonics, 12(12), 1–8. https://doi.org/10.1002/jbio.201900065

Ohnishi, S., & Takano, K. (2004). Amyloid fibrils from the viewpoint of protein folding.

Cellular and Molecular Life Sciences, 61(5), 511–524. https://doi.org/10.1007/s00018-003-3264-8

Osterhaus, A., Groen, J., Bildt, M. Van De, Martina, B., Vos, J., & Egmond, H. Van. (1997). a -Synuclein in Lewy bodies Endogenous proviruses as “mementos”? Nature, 388, 839–840.

Paravastu, A. K., Leapman, R. D., Yau, W. M., & Tycko, R. (2008). Molecular structural basis for polymorphism in Alzheimer’s β-amyloid fibrils. Proceedings of the National Academy of Sciences of the United States of America, 105(47), 18349–18354. https://doi.org/10.1073/pnas.0806270105

Petkova, A. T., Ishii, Y., Balbach, J. J., Antzutkin, O. N., Leapman, R. D., Delaglio, F., & Tycko, R. (2002). A structural model for Alzheimer’s β-amyloid fibrils based on experimental constraints from solid state NMR. Proceedings of the National Academy of Sciences of the United States of America, 99(26), 16742–16747. https://doi.org/10.1073/pnas.262663499

Petkova, A. T., Leapman, R. D., Guo, Z., Yau, W., Mark, P., Tycko, R., Petkova, A. T., Leapman, R. D., & Guo, Z. (2016). Self-Propagating, Molecular-Level Polymorphism in Alzheimer ’ s β-Amyloid Fibrils Published by : American Association for the Advancement of Science Stable URL : http://www.jstor.org/stable/3840113 REFERENCES Linked references are available on JSTOR for . 307(5707), 262–265.

Pittenger, B., Erina, N., & Su, C. (2010). Quantitative Mechanical Property Mapping at the Nanoscale with PeakForce QNM. Bruker Application Note AN128, AN128. https://doi.org/10.13140/RG.2.1.4463.8246

Riek, R., & Eisenberg, D. S. (2016). The activities of amyloids from a structural perspective.

Nature, 539(7628), 227–235. https://doi.org/10.1038/nature20416

Riihimäki-Lampén, L. H., Vainio, M. J., Vahermo, M., Pohjala, L. L., Heikura, J. M. S., Valkonen, K. H., Virtanen, V. T., Yli-Kauhaluoma, J. T., & Vuorela, P. M. (2010). The binding of synthetic retinoids to lipocalin β-lactoglobulins. Journal of Medicinal Chemistry, 53(1), 514–518. https://doi.org/10.1021/jm901309r

Ross, C. A., & Poirier, M. A. (2004). Protein aggregation and neurodegenerative disease. Nature Medicine, 10(7), S10. https://doi.org/10.1038/nm1066

Rud, V., Wir-, B., Zucker, L., Iosegewebc, C.-, Schimmer, S., Violett, S., & Snbstanz, S. (1851). Ueber eine im Gehirn und Riickenmark des Menschen aufgefumiene Substanz mit der chemischen Reaction der. 135–138.

Sakurai, K., Konuma, T., Yagi, M., & Goto, Y. (2009). Structural dynamics and folding of β-lactoglobulin probed by heteronuclear NMR. Biochimica et Biophysica Acta – General Subjects, 1790(6), 527–537. https://doi.org/10.1016/j.bbagen.2009.04.003

Sozer, N., & Kokini, J. L. (2009). Nanotechnology and its applications in the food sector. Trends in Biotechnology, 27(2), 82–89. https://doi.org/10.1016/j.tibtech.2008.10.010

Sunde, M., Serpell, L. C., Bartlam, M., Fraser, P. E., Pepys, M. B., & Blake, C. C. F. (1997). Common core structure of amyloid fibrils by synchrotron X-ray diffraction. Journal of Molecular Biology, 273(3), 729–739. https://doi.org/10.1006/jmbi.1997.1348

Tai, C. S., Chen, Y. Y., & Chen, W. L. (2016). β -Lactoglobulin Influences Human Immunity and Promotes Cell Proliferation. BioMed Research International, 2016. https://doi.org/10.1155/2016/7123587

Trojanowski, J. Q., & Revesz, T. (2007). Proposed neuropathological criteria for the post mortem diagnosis of multiple system atrophy. Neuropathology and Applied Neurobiology, 33(6), 615–620. https://doi.org/10.1111/j.1365-2990.2007.00907.x

Usov, I., Adamcik, J., & Mezzenga, R. (2013). Polymorphism complexity and handedness inversion in serum albumin amyloid fibrils. ACS Nano, 7(12), 10465–10474. https://doi.org/10.1021/nn404886k

Usov, I., & Mezzenga, R. (2015). FiberApp: An open-source software for tracking and analyzing polymers, filaments, biomacromolecules, and fibrous objects. Macromolecules, 48(5), 1269–1280. https://doi.org/10.1021/ma502264c

Volpatti, L. R., & Knowles, T. P. J. (2014). Polymer physics inspired approaches for the study of the mechanical properties of amyloid fibrils. Journal of Polymer Science, Part B: Polymer Physics, 52(4), 281–292. https://doi.org/10.1002/polb.23428

Wang, W., Nema, S., & Teagarden, D. (2010). Protein aggregation-Pathways and influencing factors. International Journal of Pharmaceutics, 390(2), 89–99. https://doi.org/10.1016/j.ijpharm.2010.02.025

Wei, G., Su, Z., Reynolds, N. P., Arosio, P., Hamley, I. W., Gazit, E., & Mezzenga, R. (2017). Self-assembling peptide and protein amyloids: From structure to tailored function in nanotechnology. Chemical Society Reviews, 46(15), 4661–4708. https://doi.org/10.1039/c6cs00542j

Zandomeneghi, G., Krebs, M. R. H., McCammon, M. G., & Fändrich, M. (2009). FTIR reveals structural differences between native β-sheet proteins and amyloid fibrils. Protein Science, 13(12), 3314–3321. https://doi.org/10.1110/ps.041024904

Zapadka, K. L., Becher, F. J., Gomes dos Santos, A. L., & Jackson, S. E. (2017). Factors affecting the physical stability (aggregation) of peptide therapeutics. Interface Focus, 7(6). https://doi.org/10.1098/rsfs.2017.0030

Zsila, F., Bikádi, Z., & Simonyi, M. (2002). Retinoic acid binding properties of the lipocalin member β-lactoglobulin studied by circular dichroism, electronic absorption spectroscopy and molecular modeling methods. Biochemical Pharmacology, 64(11), 1651–1660. https://doi.org/10.1016/S0006-2952(02)01350-3

BIOGRAPHICAL SKETCH

Santosh Khatri completed his Master of Science in Physics from University of Texas Rio Grande Valley on the spring 2020. He obtained his Bachelor of Science in Physics in 2010 and Master of Science in Physics in 2012 from Tribhuvan University, Nepal. He worked as High School teacher for 2 years in Nepal before joining UTRGV. He is interested in areas of applied physics like Biophysics and Nano-Biotechnology. His Personal email is Princeofrayale33@gmail.com.